


Suppression of quantum noise by two-mode squeezed states for photon propagation under conditions of electromagnetically induced transparency and four-wave mixing

Qi Zhang¹ and Guoxiang Huang^{1,2,3,*}

¹State Key Laboratory of Precision Spectroscopy, East China Normal University, Shanghai 200062, China

²NYU-ECNU Joint Institute of Physics, New York University at Shanghai, Shanghai 200062, China

³Collaborative Innovation Center of Extreme Optics, Shanxi University, Taiyuan, Shanxi 030006, China

 (Received 28 August 2019; revised manuscript received 5 December 2019; accepted 13 February 2020; published 5 March 2020)

Quantum vacuum noise is very detrimental for photon propagation and optical quantum memory, which particularly occurs in optically thick atomic media working under the condition of electromagnetically induced transparency (EIT) accompanied by a process of four-wave mixing (FWM). The suppression of quantum vacuum noise becomes now an imperative task for advancing the research and application of quantum memory. Here we present a scheme to suppress quantum vacuum noise and hence to improve the fidelity of photon propagation, by assuming that signal and idler laser fields are initially prepared in a two-mode squeezed vacuum state. With such a scheme, we show that the normal gain mode inherent in the EIT-based FWM system, which contributes optical gain to both the signal and idler fields, can be largely inhibited, giving rise to a significant suppression of the quantum vacuum noise along with their amplification and hence a large enhancement of the fidelity for photon propagation. The results reported here may have promising applications for high-fidelity quantum information processing and transformation, especially for improving the quality of multimode optical quantum memory based on EIT techniques.

DOI: [10.1103/PhysRevA.101.033806](https://doi.org/10.1103/PhysRevA.101.033806)

I. INTRODUCTION

Quantum memory (QM) [1–5] of photons plays a crucial role for many tasks of quantum computation and quantum information, especially for long-distance quantum communication. The basic principle of an effective QM is the use of the light-matter interaction to map single photon states into long-lived quantum matter states, which can be retrieved later on by mapping the matter states back into the photon states in a highly efficient and controllable way. One of the important methods of optical QM is based on electromagnetically induced transparency (EIT), a typical quantum destructive interference effect occurring in three-level atomic gas coupled with two laser fields (i.e., a signal field and a control field) [6]. Due to the existence of dark state polariton [7], the storage and retrieval of the signal-field photons can be realized by switching off and on of the control field successively. Since the first experimental realizations [8,9], much effort has been paid to the EIT-based schemes for optical pulse storages [10–18] and QMs [19–28].

As an important extension of the three-level scheme, EIT-based four-level ones have also been proposed as a new platform for the study of light propagation. Since the pioneering theoretical work by Zibrov *et al.* [29], much attention has been paid to the optical memory by exploiting EIT-based double- Λ -type atomic gases [30–39], aiming to find novel characters of optical memory that are absent in the

three-level one. The original suggestion of exploiting the double- Λ scheme thought that the FWM effect in such a scheme may play a positive role for optical memory; the experiment in Ref. [36] claimed that the FWM effect might be useful for such aim because the FWM provides optical gain that can be utilized to reduce the optical absorption of both the signal and idler fields, and hence to realize and enhance the storage and retrieval not only for the signal field but also for the idler field (i.e., optical memory of multimodes).

However, as pointed out in the careful experiment carried out by Phillips *et al.* [40] and in the deep theoretical analysis presented by Lauk *et al.* [41], in the EIT-based double- Λ scheme the FWM effect is very detrimental for photon propagation and for QM. The reason is that the FWM effect in such a system brings not only the optical gain but also quantum vacuum noise (QVN) to both the signal and idler fields, which lowers the fidelity of the photon propagation of the QM significantly [42]. Generally speaking, such optical gain and QVN are unavoidable for large optical depth, and hence with the EIT-based double- Λ scheme it is very difficult to realize high-fidelity photon propagation and QM [41].

In this paper, by extending the work by Lauk *et al.* [41] and generalizing the recent study [43], we suggest a scheme to suppress the gain in a double- Λ -type atomic gas, and hence to improve the fidelity of photon propagation when the system works under the conditions of EIT and FWM. We show that, if the signal and idler fields in the double- Λ atomic gas are initially prepared in a two-mode squeezed vacuum state, the normal gain mode inherent in the system (which contributes optical gain to both the signal and idler fields) can be largely

*gxhuang@phy.ecnu.edu.cn

inhibited, giving rise to a significant suppression of the QVN and hence a large enhancement of the fidelity for the photon propagation of the both signal and idler fields.

Before proceeding, we note that in recent years several approaches for suppressing the QVN in the EIT-based double- Λ systems have been reported, including the optimization of polarization selection rules [44–46], the engineering of Raman absorption using different isotopes [47], and the utilization of optical cavities [48,49]. However, our scheme is quite different from those in Refs. [44–49]. It is based on a detailed and deep analysis of two inherent normal modes (i.e., the absorption mode and gain mode) in the system, which not only shows clearly the physical reason why the QVN occurs due to FWM but also suggests us to employ a two-mode squeezed vacuum state as an input to inhibit the normal gain mode and hence the QVN (as well as its amplification) in both the signal and idler fields. In this way, the EIT-based double- Λ scheme can be used to realize high-fidelity photon propagation and multimode QM. Furthermore, the present work is also different from that in Ref. [43], where only a semiclassical approach for the suppression of the FWM was given and no quantum effect on the light propagation is considered. The research results presented here may have promising applications for high-fidelity quantum information processing and transformation, especially for optimizing and improving the quality of multimode optical QM by using EIT-based techniques.

The remainder of the paper is arranged as follows. In Sec. II, a description of full quantum model for pulse propagation is presented. In Sec. III, the propagation property of the signal and idler photons is analyzed based on a detailed normal-mode analysis. In Sec. IV, the improvement of the fidelity of photon propagation is suggested by the suppression of the normal gain mode through the input of a two-continuous-mode squeezed vacuum state for the signal and idler photons. Finally, Sec. V summarizes the main results obtained in this work and the Appendixes give calculating details omitted in the main text.

II. MODEL

We start to consider a cold, lifetime-broadened atomic gas with a double- Λ -type four-level configuration [see Fig. 1(a)],

in which $|1\rangle$ and $|2\rangle$ are two (hyperfine) ground states and $|3\rangle$ and $|4\rangle$ are two excited states. The atoms (denoted by solid black circles) are assumed to be initially prepared at the state $|1\rangle$. A signal laser field $\hat{\mathbf{E}}_S$ (with center angular frequency ω_S and wave number k_S) couples to the transition $|1\rangle \leftrightarrow |3\rangle$; a continuous-wave control laser field \mathbf{E}_c (with center angular frequency ω_c and wave number k_c) couples to the transition $|2\rangle \leftrightarrow |3\rangle$ and also the additional transition $|1\rangle \leftrightarrow |4\rangle$. Due to this additional coupling, an idler field $\hat{\mathbf{E}}_I$ (with center angular frequency ω_I and wave number k_I) will be generated via a FWM process satisfying the condition $\omega_S - \omega_c = \omega_c - \omega_I$ [40,41,43].

For simplicity and for reducing Doppler effect, all the laser fields are assumed to propagate along z direction. The control field \mathbf{E}_c is assumed to be strong enough and thus can be taken to be a classical and undepleted one, expressed by $\mathbf{E}_c = \mathbf{e}_c \mathcal{E}_c \exp(ik_c z - i\omega_c t) + \text{c.c.}$, with \mathbf{e}_c (\mathcal{E}_c) its unit polarization

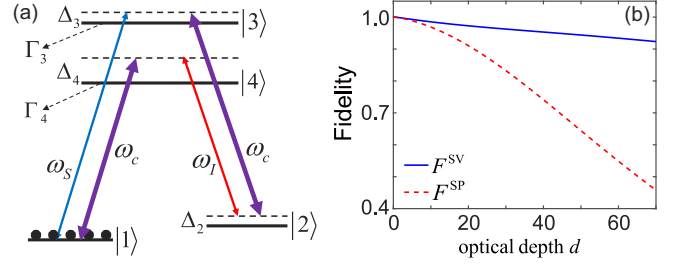


FIG. 1. (a) Energy-level diagram and excitation scheme of the EIT-based double- Λ -type atomic gas. ω_S , ω_c , and ω_I are respectively central frequencies of the signal, control, and the idler fields, Δ_α ($\alpha = 2, 3, 4$) are detunings, and Γ_α ($\alpha = 3, 4$) is the decay rate of the state $|\alpha\rangle$. Solid black circles denote atoms that are initially prepared at the ground state $|1\rangle$. (b) F^{SV} : fidelity of the photon propagation in the system as a function of optical depth d , with the input taken to be a two-mode squeezed vacuum state (solid blue line); F^{SP} : fidelity of the photon propagation, with the input taken to be a single-photon state (dashed red line).

vector (amplitude). However, the signal field $\hat{\mathbf{E}}_S$ and the idler field $\hat{\mathbf{E}}_I$ are assumed to be weak, pulsed, and quantized ones, expressed by $\hat{\mathbf{E}}_l(z, t) = \mathbf{e}_l \mathcal{E}_l \hat{a}_l(z, t) \exp(ik_l z - i\omega_l t) + \text{H.c.}$ ($l = S, I$). Here H.c. means Hermitian conjugate, \mathbf{e}_l and $\mathcal{E}_l \equiv \sqrt{\hbar\omega_l/(2c\epsilon_0 S_l)}$ (S_l is the effective cross-section area in the transverse directions) are, respectively, the unit polarization vector and the mode amplitude, and $\hat{a}_l(z, t)$ is the annihilation operator of photon of the l th field, satisfying the commutation relation $[\hat{a}_l(z, t), \hat{a}_{l'}^\dagger(z', t)] = c\delta(z - z')\delta_{ll'}$ [50].

Under electric-dipole, rotating-waving, and slowly varying envelope approximations, the Hamiltonian of the system reads

$$\begin{aligned} \hat{H}^H = & -i\hbar \int_{-\infty}^{+\infty} dz \left(\hat{a}_S^\dagger \frac{\partial}{\partial z} \hat{a}_S + \hat{a}_I^\dagger \frac{\partial}{\partial z} \hat{a}_I \right) \\ & - \hbar \mathcal{N} \int_{-\infty}^{+\infty} dz \left(\sum_{\alpha=1}^4 \Delta_\alpha \hat{S}_{\alpha\alpha} + g_S \hat{S}_{31} \hat{a}_S + \Omega_{c1} \hat{S}_{32} \right. \\ & \left. + \Omega_{c2} \hat{S}_{41} + g_I \hat{S}_{42} \hat{a}_I + \text{H.c.} \right), \end{aligned} \quad (1)$$

where \mathcal{N} is the atomic line density. Note that for obtaining the expression (1), the slowly varying atomic transition operator $\hat{S}_{\alpha\beta}(z, t) = N_z^{-1} \sum_{z_j \in \Delta_z} \hat{S}_{\alpha\beta}^j$ is introduced [7], where the averaging is made over N_z ($\gg 1$) atoms in the small spatial interval Δ_z , with $\hat{S}_{\alpha\beta}^j$ the transition operator of the atom located at z_j defined by $\hat{S}_{\alpha\beta}^j = |\alpha\rangle_j \langle\beta| \exp[i(k_\alpha - k_\beta)z_j - i(\omega_\alpha + \Delta_\alpha - \omega_\beta - \Delta_\beta)t]$. It is easy to show that $\hat{S}_{\alpha\beta}(z, t)$ satisfies the following commutation relation:

$$\begin{aligned} & [\hat{S}_{\alpha\beta}(z, t), \hat{S}_{\alpha'\beta'}(z', t)] \\ & = \mathcal{N}^{-1} \delta(z - z') [\hat{S}_{\alpha\beta'}(z, t) \delta_{\alpha'\beta} - \hat{S}_{\alpha'\beta}(z, t) \delta_{\alpha\beta'}], \end{aligned} \quad (2)$$

where $g_S \equiv (\mathbf{e}_S \cdot \mathbf{p}_{31}) \mathcal{E}_S / \hbar$ [$g_I \equiv (\mathbf{e}_I \cdot \mathbf{p}_{42}) \mathcal{E}_I / \hbar$] is the coefficient denoting the coupling between the signal (idler) field and the transition $|1\rangle \leftrightarrow |3\rangle$ ($|2\rangle \leftrightarrow |4\rangle$), $\Omega_{c1} \equiv (\mathbf{e}_c \cdot \mathbf{p}_{32}) \mathcal{E}_c / \hbar$ [$\Omega_{c2} \equiv (\mathbf{e}_c \cdot \mathbf{p}_{41}) \mathcal{E}_c / \hbar$] is the half Rabi frequency related to the control field coupling to the transition $|2\rangle \leftrightarrow |3\rangle$ ($|1\rangle \leftrightarrow |4\rangle$), with $\mathbf{p}_{\alpha\beta}$ the electric-dipole matrix element associated

with the transition $|\alpha\rangle \leftrightarrow |\beta\rangle$; $\Delta_2 = \omega_c - \omega_I - (E_2 - E_1)/\hbar$, $\Delta_3 = \omega_S - (E_3 - E_1)/\hbar$, and $\Delta_4 = \omega_c - (E_4 - E_1)/\hbar$ are detunings, with $E_\alpha = \hbar\omega_\alpha$ the eigenenergy of the state $|\alpha\rangle$.

The dynamics of the system is governed by Heisenberg-Langevin and Maxwell equations, which are given by

$$\begin{aligned} \frac{\partial}{\partial t} \hat{S}_{\alpha\beta}(z, t) \\ = -\frac{i}{\hbar} [\hat{S}_{\alpha\beta}(z, t), \hat{H}^H] - \Gamma(\hat{S}_{\alpha\beta}) + \hat{F}_{\alpha\beta}(z, t), \end{aligned} \quad (3a)$$

$$i\left(\frac{\partial}{\partial z} + \frac{1}{c} \frac{\partial}{\partial t}\right) \hat{a}_S(z, t) + g_S^* \mathcal{N} \hat{S}_{13}(z, t) = 0, \quad (3b)$$

$$i\left(\frac{\partial}{\partial z} + \frac{1}{c} \frac{\partial}{\partial t}\right) \hat{a}_I^\dagger(z, t) - g_I \mathcal{N} \hat{S}_{42}(z, t) = 0, \quad (3c)$$

where Γ is the 4×4 relaxation matrix describing the spontaneous emission and dephasing in the atomic system and $\hat{F}_{\alpha\beta}(z, t)$ is the δ -correlated Langevin noise operator, introduced to keep the commutation relations of the operators $\hat{S}_{\alpha\beta}$. An explicit expression of Eq. (3a) is presented in Appendix A.

The theoretical model described above [Fig. 1(a)] can be easily realized by experiment. One of the candidates is the laser-cooled alkali ^{87}Rb atomic gas interacting with the control field \mathbf{E}_c , the signal field $\hat{\mathbf{E}}_S$, and the idler field $\hat{\mathbf{E}}_I$, with the atomic levels chosen to be $|1\rangle = |5^2S_{1/2}, F=1, m_F=1\rangle$, $|2\rangle = |5^2S_{1/2}, F=2, m_F=2\rangle$, $|3\rangle = |5^2P_{3/2}, F=2, m_F=2\rangle$, and $|4\rangle = |5^2P_{3/2}, F=2, m_F=1\rangle$ [38,40,51]. System parameters used in the following calculations are given by $\Gamma_{12} = 2\pi \times 1$ kHz and $\Gamma_{13} = \Gamma_{23} = \Gamma_{14} = \Gamma_{24} = 2\pi \times 3$ MHz.

III. PROPAGATION PROPERTY OF THE SIGNAL AND IDLER PHOTONS

Now we turn to considering the physical property of the FWM, which occurs during the propagation and QM processes of the signal and idler fields when the control field is switched on in the system. Due to the FWM, both the signal and idler fields acquire gain. Superficially, such gain may be advantageous not only for the propagation but also for the memory of the signal and idler fields since it can be employed to suppress the optical absorption. However, the gain will also result in the generation of QVN photons, which will be amplified during propagation and hence make both the signal and idler fields distort and lower the fidelity of the photon propagation and the QM. Although such conclusion has been obtained or implied in Ref. [41], here we give a different approach, i.e., normal-mode analysis, by which the physical reason why the QVN occurs and why they are amplified rapidly in the system can be seen and understood in a transparent way.

A. Normal mode solutions and their physical properties

The normal mode solutions of the Heisenberg-Langevin-Maxwell equations (3a)–(3c) with an all-quantum approach can be carried out in the following way. First, we seek the zero-order solution (also called base state, i.e., the steady state when the signal and the idler fields are absent) of Eqs. (3a)–(3c) by assuming the control field to be constant (i.e., Ω_{c1} and Ω_{c2} are constants), with the result given in

Appendix B. We see that, for a small or intermediate value of the one-photon detuning Δ_4 , the atoms populate in all four inner states, which is not desirable because the signal and idler fields will get a large gain during time evolution; however, if Δ_4 is large, nearly all the atoms populate in the ground state $|1\rangle$, which makes the gain become small. For simplicity, in the following calculations we assume that Δ_4 takes a large value approximately equaling the frequency difference between $|1\rangle$ and $|2\rangle$, i.e., $\Delta_4 \approx (E_2 - E_1)/\hbar$. Under such a condition, the zero-order solution of Eqs. (3a)–(3c) is reduced into $\hat{S}_{11}^{(0)} \approx \hat{I}$ and $\hat{S}_{14}^{(0)} \approx -\delta \hat{I}$, with other $\hat{S}_{\alpha\beta}^{(0)} \approx 0$. Here $\delta \equiv \Omega_{c2}/\Delta_4$ and \hat{I} is the identity operator (see Appendix B for details).

We assume that there are only small photon numbers in the signal and idler fields. In this case, the linear excitation solution around the base state [i.e., first-order solution of the Heisenberg-Langevin-Maxwell equations (3a)–(3c)] is enough to give a reasonable description of the time evolution of the system. By taking $\hat{S}_{\alpha\beta} \rightarrow \hat{S}_{\alpha\beta}^{(0)} + \hat{S}_{\alpha\beta}$, Eq. (3a) can be linearized, which, together with the Maxwell equations (3b) and (3c), can be solved exactly by using a Fourier transform. After eliminating the atomic variables, we obtain the closed equations for \tilde{a}_S and \tilde{a}_I^\dagger as follows:

$$\begin{aligned} -i \frac{\partial}{\partial z} \begin{bmatrix} \tilde{a}_S \\ \tilde{a}_I^\dagger \end{bmatrix} = \begin{bmatrix} \frac{\omega}{c} + \mathcal{N} |g_S|^2 \frac{\omega + D_{21}}{D} & \mathcal{N} \delta g_I^* g_S \frac{\Omega_{c1}}{D} \\ -\mathcal{N} \delta^* g_I g_S \frac{\Omega_{c1}}{D} & \frac{\omega}{c} - \mathcal{N} |\delta g_I|^2 \frac{\omega + D_{31}}{D} \end{bmatrix} \begin{bmatrix} \tilde{a}_S \\ \tilde{a}_I^\dagger \end{bmatrix} \\ - i \mathcal{N} \begin{bmatrix} -g_S^* \frac{\Omega_{c1}}{D} \\ \delta^* g_I \frac{\omega + D_{31}}{D} \end{bmatrix} \tilde{F}_{12} - i \mathcal{N} \begin{bmatrix} g_S^* \frac{\omega + D_{21}}{D} \\ \delta^* g_I \frac{-\Omega_{c1}}{D} \end{bmatrix} \tilde{F}_{13}, \end{aligned} \quad (4)$$

with $D(\omega) = |\Omega_{c1}|^2 - (\omega + D_{21})(\omega + D_{31})$ and $D_{\alpha 1} = d_{\alpha 1} + |\Omega_{c2}|^2/\Delta_4$. Here $\tilde{a}_S(z, \omega)$ and $\tilde{a}_I^\dagger(z, \omega)$ are respectively Fourier transforms of $\hat{a}_S(z, t)$ and $\hat{a}_I^\dagger(z, t)$, satisfying the commutation relation $[\tilde{a}_I(z, \omega), \tilde{a}_I^\dagger(z, \omega')] = \delta_{I I'} \delta(\omega - \omega')$ [52]. For more detail, see Appendix B.

The solution of the above linear coupled equations reads

$$\tilde{a}_S(z, \omega) = \tilde{c}_+(z, \omega) e^{iK_+(\omega)z} + \tilde{c}_-(z, \omega) e^{iK_-(\omega)z}, \quad (5a)$$

$$\tilde{a}_I^\dagger(z, \omega) = G_+(\omega) \tilde{c}_+(z, \omega) e^{iK_+(\omega)z} + G_-(\omega) \tilde{c}_-(z, \omega) e^{iK_-(\omega)z}, \quad (5b)$$

where

$$\begin{aligned} \tilde{c}_\pm(z, \omega) \\ = \frac{\tilde{a}_I^\dagger(0, \omega) - G_\mp(\omega) \tilde{a}_S(0, \omega)}{G_\pm(\omega) - G_\mp(\omega)} \\ + \frac{\mathcal{N}}{D} \int_0^z dz' \left\{ \frac{\delta^* g_I (\omega + D_{31}) + g_S^* G_\mp(\omega) \Omega_{c1}}{G_\pm(\omega) - G_\mp(\omega)} \tilde{F}_{12}(z', \omega) \right. \\ \left. - \frac{\delta^* g_I \Omega_{c1}^* + g_S^* G_\mp(\omega) (\omega + D_{21})}{G_\pm(\omega) - G_\mp(\omega)} \tilde{F}_{13}(z', \omega) \right\} e^{-iK_\pm(\omega)z'} \end{aligned} \quad (6)$$

are superposition coefficients, with $G_\pm \equiv (-D_\pm \pm \sqrt{D_\pm^2 - 4|\delta g_I g_S|^2 |\Omega_{c1}|^2}) / (2\delta g_I^* g_S^* \Omega_{c1})$ and $D_\pm \equiv (\omega + D_{21}) |g_S|^2 \pm (\omega + D_{31}) |\delta g_I|^2$. The solution (5) can also be expressed in terms of the boundary values $\tilde{a}_S(0, \omega)$ and $\tilde{a}_I^\dagger(0, \omega)$, which is presented in Appendix C.

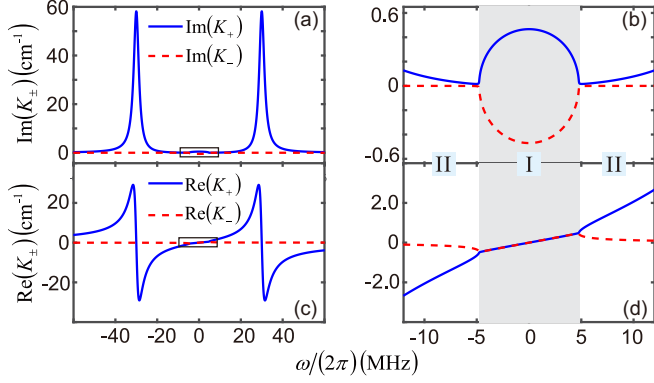


FIG. 2. Linear dispersion relations of the two normal modes, i.e., the absorption mode K_+ and the gain mode K_- , as functions of ω . (a) Solid blue line: $\text{Im}(K_+)$; dashed red line: $\text{Im}(K_-)$. (b) The zoomed detail of the small solid black rectangle plotted near $\omega = 0$ of panel (a), which is divided into region I (middle shadow area) and region II (the one except for the shadow area). The solid blue line is for $\text{Im}(K_+)$ and the dashed red line is for $\text{Im}(K_-)$. A remarkable character is the existence of the “bubble” in the region I, where the K_+ (K_-) mode has a significant absorption (gain). Outside of the bubble (i.e., the region II), the absorption (gain) for the K_+ (K_-) mode is small. (c) Solid blue line: $\text{Re}(K_+)$; dashed red line: $\text{Re}(K_-)$. (d) The zoomed detail of the small solid black rectangle plotted near $\omega = 0$ of panel (c), which is also divided into regions I and II, corresponding to those in panel (b). The solid blue (dashed red) line is for $\text{Re}(K_+)$ [$\text{Re}(K_-)$]. A remarkable character here is the existence of two “coincident straight lines” in the region I, which means that both the K_+ and K_- modes have normal dispersion and hence slow group velocity. However, in the region II, K_+ (K_-) mode has normal (abnormal) dispersion.

From the expression (5) we see that the solution of both the signal and idler fields contains two parts, connected by the superposition coefficients $\tilde{\delta}_\pm(z, \omega)$. K_+ and K_- in the solution are linear dispersion relations, given by

$$K_\pm(\omega) = \frac{\omega}{c} + \frac{\mathcal{N}}{2D(\omega)} [D_-(\omega) \pm \sqrt{D_+^2(\omega) - 4|\delta g_I g_S|^2 |\Omega_{c1}|^2}], \quad (7)$$

which means that the photon propagations of the signal and idler fields can be characterized by two inherent *normal modes* (called K_+ mode and K_- mode below). Obviously, similar to those obtained in a system with two coupled harmonic oscillators, these normal modes possess features of collective excitations, deserving to be analyzed in more detail.

Shown in Fig. 2 are linear dispersion relations of the K_+ mode (solid blue line) and K_- mode (dashed red line) as functions of ω . When plotting the figure, a set of realistic physical parameters were taken, given by $\Delta_4 = 2\pi \times 150$ MHz, $\Delta_2 = \Delta_3 = 0$, $|\Omega_{c1}| = 2\pi \times 30$ MHz, $|\Omega_{c2}| = 2\pi \times 17$ MHz, and $|g_S|^2 \mathcal{N} = |g_I|^2 \mathcal{N} = 1.1 \times 10^9 \text{ cm}^{-1} \text{ s}^{-1}$. The solid blue line in panel (a) is the imaginary part of K_+ mode, i.e., $\text{Im}(K_+)$; the dashed red line is the imaginary part of K_- mode, i.e., $\text{Im}(K_-)$. Obviously, K_+ mode is an absorption mode because $\text{Im}(K_+) > 0$, while K_- mode is a gain mode because $\text{Im}(K_-) < 0$. The appearance of the gain mode is due to the FWM effect, which disappears when $\delta = \Omega_{c2}/\Delta_4 \rightarrow 0$.

Shown in panel (b) is the zoomed detail of the small solid black rectangle plotted near $\omega = 0$ of panel (a), which is divided into region I (middle shadow area) and region II (i.e., the one except for region I). The solid blue line is for $\text{Im}(K_+)$ and the dashed red line is for $\text{Im}(K_-)$. A remarkable character here is the existence of the “bubble” in region I, where the K_+ mode (K_- mode) has a significant absorption (gain), while, outside of the bubble (i.e., region II), the absorption (gain) for the K_+ (K_-) mode is small.

The solid blue line in panel (c) shows $\text{Re}(K_+)$ (the real part of K_+) and the dashed red line shows $\text{Re}(K_-)$ (the real part of K_-). Their details near the region $\omega = 0$ (i.e., the small solid black rectangle plotted in this panel) are illustrated by panel (d), which is also divided into regions I and II, exactly corresponding to those in panel (b). The solid blue (dashed red) line in the figure is for $\text{Re}(K_+)$ [$\text{Re}(K_-)$]. A remarkable character here is the existence of the two “coincident straight lines” in region I, which means that in this region both the K_+ and K_- modes have normal dispersion and their group velocities can be slowed down simultaneously. However, in region II, K_+ (K_-) mode has normal (abnormal) dispersion [53]. This remarkable character of the K_+ and K_- modes may have deep implication and be useful not only for EIT-based QM but also for biphoton generation by using the atomic spontaneous FWM considered in Refs. [28,54–57].

The occurrence of the bubble in Fig. 2(b) and the coincident straight lines in Fig. 2(d) can be understood as follows. For large Δ_4 (or small δ) and small ω , the linear dispersion relations (7) are reduced into the form

$$K_\pm(\omega) \approx \frac{\omega}{c} + \frac{\mathcal{N}}{2D(\omega)} [\omega \pm i\sqrt{4|\delta g_I g_S|^2 |\Omega_{c1}|^2 - \omega^2}], \quad (8)$$

with $4|\delta g_I g_S|^2 |\Omega_{c1}|^2 - \omega^2 \geq 0$, i.e., in this case K_+ and K_- are complex conjugate of each other, which gives the results $\text{Im}(K_+) = -\text{Im}(K_-)$ and $\text{Re}(K_+) = \text{Re}(K_-)$. Physically, such results come from the fact that, for the large Δ_4 (or small δ) and small ω , the system works essentially in the EIT regime so both the K_+ mode and K_- mode have normal dispersion (and hence slow group velocity $V_g^+|_{\omega=0} \approx V_g^-|_{\omega=0} = 2.2 \times 10^{-3} c$), but they experience respectively absorption and gain due to the existence of a small Raman gain in the system.

The property of the linear dispersion relations of the two normal modes as functions of ω for Δ_4 is also studied. The result shows that the propagation of the signal and idler fields in this situation possesses some rich features not present for the case of large Δ_4 . For detail, see Appendix D.

B. Propagation of the signal and idler fields with input of a single-photon state

We now consider the propagation of the signal and idler photons in the system for the case of large Δ_4 . First, we assume that on the left boundary of the atomic medium ($z = 0$) the input signal field is in a state of single-photon wave packet, while the idler field is in a vacuum state. So the quantum state of the total input light field can be expressed as

$$|\Psi^{\text{SP}}\rangle = \int_{-\infty}^{+\infty} d\omega f_S(\omega) \hat{a}_S^\dagger(0, \omega) |0_S\rangle, |0_I\rangle, \quad (9)$$

where ‘‘SP’’ means single photon, $|\{0_S\}, \{0_I\}\rangle = |\{0_S\}\rangle \otimes |\{0_I\}\rangle$ is the vacuum state with no signal and idler photon, and $f_S(\omega) = (\Delta\omega_S\sqrt{\pi})^{-1/2} \exp[-\omega^2/(2\Delta\omega_S^2)]$ is a normalized mode distribution function, with $\Delta\omega_S$ characterizing its width.

We are interested in the variation of photon numbers of the signal and idler fields during propagation in the atomic gas, which, as functions of the propagation distance z , are defined by [58]

$$n_j^{\text{SP}}(z) \equiv \int_{-\infty}^{+\infty} dt \langle \Psi^{\text{SP}} | \hat{a}_j^\dagger(z, t) \hat{a}_j(z, t) | \Psi^{\text{SP}} \rangle, \quad (10)$$

with $j = S, I$. The single-photon state (9) ensures that the photon number of the input signal (idler) field $n_S(0) = 1$ [$n_I(0) = 0$]. The photon numbers of the signal and idler fields at position z can be obtained by substituting the expressions (5) and (9) into the formula (10). Then we obtain the photon number of the signal field

$$n_S^{\text{SP}}(z) = n_{S1}(z) + n_{S2}(z) + n_{S10}(z), \quad (11a)$$

$$n_{S1}(z) = \int_{-\infty}^{+\infty} d\omega |C_{SS}(z, \omega) f_S(\omega)|^2, \quad (11b)$$

$$n_{S2}(z) = \int_{-\infty}^{+\infty} \frac{d\omega}{\sqrt{2\pi}} \int_0^z dz' |C_{S12}(z - z', \omega)|^2 \Gamma_{23} \langle \tilde{\hat{S}}_{33}(z', 0) \rangle, \quad (11c)$$

$$n_{S10}(z) = \frac{1}{\Delta\omega_S} \int_{-\infty}^{+\infty} \frac{d\omega}{2\pi} |C_{SI}(z, \omega)|^2, \quad (11d)$$

where n_{S1} is contributed from the nonzero input of the signal field (which exists in the semiclassical solution) and n_{S2} is due to the Langevin (i.e., spontaneous-emission) noise. However, the term n_{S10} comes from QVN, which appears purely due to the quantum character of the signal field [59]. The photon number of the signal field is given by

$$n_I^{\text{SP}}(z) = n_{I1}(z) + n_{I2}(z) + n_{I10}(z) + n_{I20}(z), \quad (12a)$$

$$n_{I1}(z) = \int_{-\infty}^{+\infty} d\omega |C_{IS}(z, \omega) f_S(\omega)|^2, \quad (12b)$$

$$n_{I2}(z) = \int_{-\infty}^{+\infty} \frac{d\omega}{\sqrt{2\pi}} \int_0^z dz' \{ |C_{I13}(z - z', \omega)|^2 \times [(\Gamma_{12} - \Gamma_3) \langle \tilde{\hat{S}}_{22}(z', 0) \rangle - \Gamma_{23} \langle \tilde{\hat{S}}_{33}(z', 0) \rangle] + |C_{I12}(z - z', \omega)|^2 (\Gamma_{13} - \Gamma_{12}) \langle \tilde{\hat{S}}_{33}(z', 0) \rangle \}, \quad (12c)$$

$$n_{I10}(z) = \frac{1}{\Delta\omega_S} \int_{-\infty}^{+\infty} \frac{d\omega}{2\pi} |C_{IS}(z, \omega)|^2, \quad (12d)$$

$$n_{I20}(z) = \frac{1}{\Delta\omega_S} \int_{-\infty}^{+\infty} \frac{d\omega}{2\pi} \int_0^z dz' [|C_{I12}(z - z', \omega)|^2 \Gamma_{12} + |C_{I13}(z - z', \omega)|^2 \Gamma_3], \quad (12e)$$

where n_{I1} is contributed from the nonzero input of the signal field, n_{I2} is due to the Langevin noise, and n_{I10} results from the QVN of the idler field [59]. Note that, different from the signal field, there is an additional term appearing in the idler field, i.e., n_{I20} , which is contributed from the ground-state population. In the formulas (11) and (12), explicit expressions

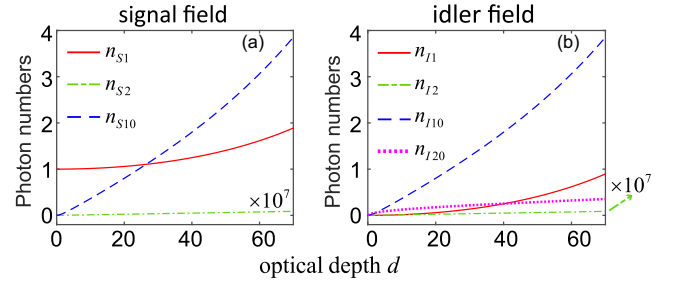


FIG. 3. Photon numbers of the signal and idler fields as functions of optical depth d , via the input of the single-photon state (9). (a) Photon number of the signal field $n_S^{\text{SP}} \equiv n_{S1} + n_{S2} + n_{S10}$: n_{S1} : photon number contributed by the nonzero input of the signal field (solid red line); n_{S2} : photon number contributed by the Langevin noise (multiplied by 10^7), denoted by dashed-dotted green line; n_{S10} : photon number contributed by the QVN (dashed blue line). (b) Photon number of the idler field $n_I^{\text{SP}} \equiv n_{I1} + n_{I2} + n_{I10} + n_{I20}$: n_{I1} : photon number due to the nonzero input of the signal field (solid red line); n_{I2} : photon number due to the Langevin noise (multiplied by 10^7 ; dashed-dotted green line); n_{I10} : photon number due to the QVN (dashed blue line); n_{I20} : photon number due to the ground-state population (dotted red line). Note that, for both the signal and idler fields, the photon numbers produced by the Langevin noise are very small, but the photon numbers produced by the QVN grow very rapidly.

of C_{SS} , C_{SI} , C_{S12} , C_{IS} , C_{I12} , and C_{I13} are presented in Appendix C. However, explicit expressions of the Fourier transform of $\hat{S}_{\alpha\beta}(z, t)$, i.e., $\hat{S}_{\alpha\beta}(z, \omega)$ ($\alpha, \beta = 2, 3$), are lengthy and thus omitted here.

Illustrated in Fig. 3 are photon numbers of the signal and idler fields as functions of the optical depth d ($\equiv \mathcal{N}|g_S|^2 z/\gamma_{31}$) of the atomic gas, when the system works in region I of Figs. 2(b) and 2(d). Panel (a) shows the photon number of the signal field $n_S^{\text{SP}} \equiv n_{S1} + n_{S2} + n_{S10}$, with n_{S1} (the photon number contributed by the nonzero input of the signal field), n_{S2} (the photon number due to the Langevin noise), and n_{S10} (the photon number due to the QVN) plotted by solid red line, dashed-dotted green line, and dashed blue line, respectively. We see that the photon number produced by the Langevin noise is very small (when plotting the figure an amplification of 10^7 times is used), but the photon numbers produced by the QVN grow exponentially. Note that, when plotting the figure, we have taken $\Delta_2 = \Delta_3 = 0$ and $\Delta\omega_S = 0.3\gamma_{31}$, with other parameters the same as those used in Fig. 2. The maximum value of d in Fig. 2 is chosen to be 70, corresponding to the length of the atomic medium $L \approx 1.2$ cm, for which the validity of the perturbation approach of the FWM effect is ensured.

Panel (b) shows the photon number of the idler field $n_I^{\text{SP}} \equiv n_{I1} + n_{I2} + n_{I10} + n_{I20}$, with n_{I1} (the photon number contributed by the nonzero input of the signal field), n_{I2} (the photon number due to the Langevin noise), n_{I10} (the photon number due to the QVN), and n_{I20} (the photon number due to the ground-state population) plotted by solid red line, dashed-dotted green line, dashed blue line, and dotted red line, respectively. We see also that the photon number produced by the Langevin noise is very small and the photon numbers produced by the QVN grow very rapidly.

Based on the results obtained in Fig. 3, we can arrive at the following conclusions. (i) The the nonzero input of the signal field, Langevin noise, QVN, and ground-state population contribute to the photon numbers of both the signal and idler fields, and these photon numbers increase during propagation. Among them, growth of the photon number by the QVN is the fastest one. The physical reason for the increased photon number is due to the existence of the K_- normal mode in the system, which provides a gain and thus an amplification to both the signal and idler fields. This point can be clearly seen by the factor e^{iK_-z} appearing in the expressions (C2a)–(C2f) of Appendix C. (ii) Among all the photon numbers, n_{S10} and n_{I10} (i.e., photon numbers due to QVN) have the fastest growth rates, which means the input signal photon will be inevitably drowned in the QVN photons even at a short propagation distance. As a result, the fidelity of the signal photon propagation will be largely reduced, and hence a quantum information processing (e.g., the QM of the signal photon) is impossible [41]. (iii) Compared with the contribution from the nonzero input and the QVN, for large Δ_4 the photon numbers produced from the Langevin noise and by the ground-state population are very small and hence can be safely neglected.

IV. SUPPRESSION OF THE GAIN MODE AND IMPROVEMENT OF THE FIDELITY FOR PHOTON PROPAGATION

From the discussion given above, we see that the QVN due to the K_- gain mode is very detrimental for quantum information processing. Thus it is desirable to seek suitable methods to inhibit such gain mode and hence the QVN. In the following, we propose a technique to suppress the gain mode and hence improve the fidelity of the photon propagation for both the signal and idler fields.

A. Suppression of the gain mode

By inspecting the result given by (5), we see that, to suppress the QVN and also its growth, a direct way is to find an input photon quantum state $|\Psi\rangle$ to make $\tilde{c}_-(0, \omega)|\Psi\rangle = 0$, so that the role played by the normal gain mode (i.e., K_- mode) is inhibited at the input of the system. This can be achieved in the following way. We assume that, for a given ω , the light field at the input position $z = 0$ is in a two-mode [60] quantum state, satisfying the condition $\tilde{c}_-(0, \omega)|\Psi\rangle = 0$, i.e., $[\hat{a}_I^\dagger(0, \omega) - |G_+| \exp(i\phi_+) \tilde{a}_S(0, \omega)]|\Psi\rangle = 0$, with $G_+(\omega) \equiv |G_+(\omega)| \exp[i\phi_+(\omega)]$. This condition can be rewritten into the following form:

$$[\hat{L}_0(\omega) + \hat{L}_1(\omega)]|\Psi\rangle = 0, \quad (13)$$

where $\hat{L}_0 = \tilde{a}_I^\dagger(0, \omega) - |\tilde{G}_+(\omega)| \exp[i\phi_+(\omega)] \tilde{a}_S(0, \omega)$ and $\hat{L}_1 = \epsilon(\omega) \exp(i\phi_+) \tilde{a}_S(0, \omega)$ are operators, $\epsilon(\omega)$ is a ω -dependent parameter, and $|\tilde{G}_+| \equiv |G_+| + \epsilon(\omega)$.

When ϵ is small, Eq. (13) can be solved by using the perturbation expansion $|\Psi\rangle = |\Psi\rangle^{(0)} + |\Psi\rangle^{(1)} + \dots$. At the leading order, one has $\hat{L}_0|\Psi\rangle^{(0)} = 0$, i.e.,

$$[\tilde{a}_I^\dagger(0, \omega) + |\tilde{G}_+(\omega)| e^{-i[\pi - \phi_+(\omega)]} \tilde{a}_S(0, \omega)]|\Psi\rangle^{(0)} = 0. \quad (14)$$

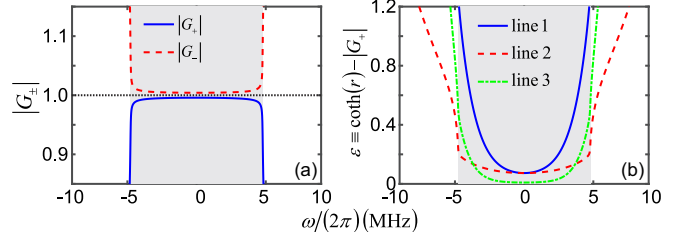


FIG. 4. (a) $|G_+|$ (solid blue line) and $|G_-|$ (dashed red line) as a function of ω . (b) $\epsilon \equiv \coth r - |G_+|$ as a function of ω for three sets of (A, ω_d) . Line 1 (solid blue line): $(A, \omega_d) = (1.7, 1.0 \Gamma_{13})$; line 2 (dashed red line): $(A, \omega_d) = (1.7, 2.0 \Gamma_{13})$; line 3 (dashed-dotted green line): $(A, \omega_d) = (3.0, 1.0 \Gamma_{13})$.

Remarkably, this equation has the same form as that of the eigenequation of a two-mode squeezed vacuum state [58,61]. Thus we obtain the solution $|\Psi\rangle^{(0)} = e^{\hat{P}_2 - \hat{P}_2^\dagger} |\{0_S\}, \{0_I\}\rangle$, where $\hat{P}_2^\dagger \equiv \xi(\omega) \tilde{a}_S^\dagger(0, \omega) \tilde{a}_I^\dagger(0, -\omega)$, and $\xi(\omega) = r(\omega) \exp[i\theta(\omega)]$ is the squeezing parameter, with r the amplitude characterizing the squeezing degree and θ the phase characterizing the squeezing direction. After a simple comparison with the standard eigenequation of a two-mode squeezed vacuum state [62], these two parameters can be readily specified as

$$\coth r = |\tilde{G}_+| \equiv |G_+| + \epsilon, \quad (15a)$$

$$\theta = \pi - \phi_+. \quad (15b)$$

Equation (15b) indicates that the input two-mode squeezed vacuum state must be phase modulated.

To ensure Eq. (14) possesses indeed the solution of two-mode squeezed vacuum state, the condition $|\tilde{G}_+| \equiv |G_+| + \epsilon \geq 1$ must be satisfied. Shown in Fig. 4(a) are $|G_\pm|$ as functions of ω based on the system parameters used in Fig. 2. We see that though $|G_+| \leq 1$ for all ω , it is very close to unity inside the shadow area [i.e., the region I of Figs. 2(b) and 2(d)]. If a positive ϵ can be chosen to make $|\tilde{G}_+| \equiv |G_+| + \epsilon \geq 1$, the eigenequation of the two-mode squeezed vacuum state obeying Eq. (14) might give the leading-order solution (13). So the problem is converted into how to find a suitable scheme to determine the parameter ϵ .

To determine ϵ , we assume the mode distribution of the squeezed vacuum state, i.e., $r(\omega)$, is a Gaussian of the form $r(\omega) = A \exp[-\omega^2/(2\omega_d^2)]$, where A is the squeezing amplitude and ω_d is the squeezing width. With this and based on the formula (15a), we can calculate the value of ϵ . Shown in Fig. 4(b) is $\epsilon \equiv \coth(r) - |G_+|$ as a function of ω for three sets of the parameters A and ω_d , where line 1 (solid blue line) is for $(A, \omega_d) = (1.7, 1.0 \Gamma_{13})$, line 2 (dashed red line) is for $(A, \omega_d) = (1.7, 2.0 \Gamma_{13})$, and line 3 (dashed-dotted green line) is for $(A, \omega_d) = (3.0, 1.0 \Gamma_{13})$. We have the following conclusions: (i) for all the three curves, $\epsilon \ll 1$ is always satisfied in the domain near $\omega = 0$; (ii) the frequency region for $\epsilon \ll 1$ is enlarged as ω_d increases (see lines 1 and 2 in the figure).

The result given above indicates that the parameter ϵ can be determined and the condition $0 < \epsilon \ll 1$ can be indeed achieved by inputting the two-mode squeezed vacuum state with the squeezing degree $r(\omega)$ of a broad frequency distribution (i.e., large ω_d) and a moderate amplitude A , which may

ensure the validity of the perturbation expansion for solving Eq. (13). The higher-order modifications to the leading-order solution of this equation can be obtained easily, which are small and lengthy and hence omitted here.

B. Improvement of the fidelity of photon propagations for both the signal and idler fields

In the last subsection, we have shown that the two-mode squeezed vacuum state satisfying Eq. (13) can be used to suppress the K_- gain mode appearing in both the signal and idler fields for the case with only a single-frequency component (i.e., ω is fixed).

Obviously, due to the linear character of Eq. (4), the result obtained there can be easily generalized to the situation where the signal and the idler fields contain multiple-frequency components. Consequently, to suppress the K_- gain mode for any ω in the pulses, one can assume that the input signal and the idler fields is in a two-continuous-mode squeezed vacuum state [63], with the following form:

$$|\Psi^{\text{SV}}\rangle = \exp \left\{ \int_{-\infty}^{+\infty} d\omega [\xi^*(\omega) \tilde{a}_S(0, \omega) \tilde{a}_I(0, -\omega) - \xi(\omega) \tilde{a}_S^\dagger(0, \omega) \tilde{a}_I^\dagger(0, -\omega)] \right\} | \{0_S\}, \{0_I\} \rangle, \quad (16)$$

where ‘‘SV’’ means the squeezed vacuum state. Such two-continuous-mode squeezed vacuum state may be generated by the nondegenerate spontaneous parametric down-conversion (SPDC) [58] using a nearly monochromatic pump beam [64].

It is expected that, with the input state (16), the QVN for different ω in the system will be suppressed significantly. To prove this, we give an analysis on the variation of the photon numbers in the signal and idler fields as their input is in the two-continuous-mode squeezed vacuum state (16) and propagates along the z direction in the atomic ensemble. Similar to (10), these photon numbers are defined by

$$n_j^{\text{SV}}(z) \equiv \int_{-\infty}^{+\infty} dt \langle \Psi^{\text{SV}} | \hat{a}_j^\dagger(z_j, t) \hat{a}_j(z_j, t) | \Psi^{\text{SV}} \rangle, \quad (17)$$

with $j = S, I$. By substituting the solution (5) [with (6)] and the input state (16) into the above formula, we obtain the result of the photon numbers of the signal and the idler fields as functions of position z , given respectively by

$$n_S^{\text{SV}}(z) = \frac{1}{\Delta\omega_S} I_S^{\text{SV}}(z), \quad (18a)$$

$$I_S^{\text{SV}}(z) = \int_{-\infty}^{+\infty} \frac{d\omega}{2\pi} |C_{SI}(z, \omega) \cosh r(\omega) - C_{SS}(z, \omega) e^{i\theta(\omega)} \sinh r(\omega)|^2, \quad (18b)$$

$$n_I^{\text{SV}}(z) = \frac{1}{\Delta\omega_S} I_I^{\text{SV}}(z), \quad (18c)$$

$$I_I^{\text{SV}}(z) = \int_{-\infty}^{+\infty} \frac{d\omega}{2\pi} |C_{IS}(z, \omega) \cosh r(\omega) - C_{II}(z, \omega) e^{-i\theta(\omega)} \sinh r(\omega)|^2, \quad (18d)$$

where concrete expressions of C_{SI} , C_{SS} , C_{IS} , and C_{II} are presented in Appendix C. Note that when obtaining the above expressions, the small contribution from the Langevin noise

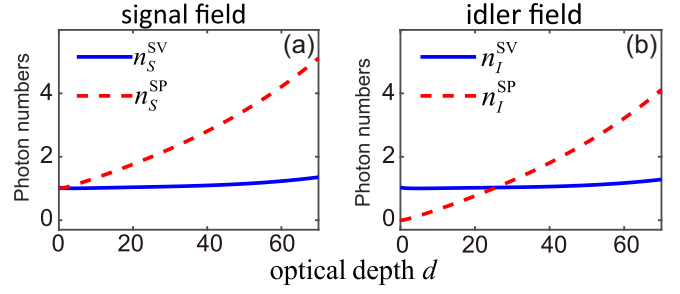


FIG. 5. Photon numbers of the signal and idler fields as functions of optical depth d , via the input of the two-continuous-mode squeezed vacuum state (16). (a) n_S^{SV} : photon number of the signal field (solid blue line). n_S^{SP} : photon number of the signal field via the input of the single-photon state (9) (dashed red line). (b) n_I^{SV} : photon number of the idler field (solid blue line). n_I^{SP} : photon number of the idler field via the input of the single-photon state (9) (dashed red line). Note that, for both the signal and idler fields, the changes of the photon numbers with the optical depth d by using the input of the two-continuous-mode squeezed state are much lower than the those by using the input of the single-photon state (9).

has been neglected. In addition, since the signal and the idler fields are continuous waves, their photon numbers, i.e., Eqs. (18a) and (18c), have been calculated by specifying a time width for detection. In the calculation, this time width is assumed to equal the time duration of the single-photon wave packets, i.e., $1/\Delta\omega_S$. The calculation of the photon numbers for the case of the pulsed signal and the idler fields has also been carried out; see Appendix E for detail.

Shown in Fig. 5 is the numerical result of the photon numbers of the signal and idler fields as functions of optical depth d when the input of the two light fields is taken to be the two-continuous-mode squeezed vacuum state (16). The solid blue line in Fig. 5(a) is the photon number of the signal field, i.e., n_S^{SV} . For comparison, the photon number of the signal field via the input of the single photon state (9), i.e., n_S^{SP} , is also illustrated by dashed red line. Similarly, the solid blue line in Fig. 5(b) is the photon number of the idler field, i.e., n_I^{SV} ; the dashed red line is the photon number of the idler field, i.e., n_I^{SP} , via the input of the single photon state (9). When plotting the figure, we have taken $f_S = (0.3\sqrt{\pi}\gamma_{31})^{-1/2} \exp[-\omega^2/(0.18\gamma_{31}^2)]$ for the single photon input state and $r = 0.7 \exp[-\omega^2/(8\gamma_{31}^2)]$ for the two-continuous-mode squeezed vacuum input state. Other system parameters are the same as those used in Fig. 2.

From Fig. 5 we see that, with the use of the input of the two-continuous-mode squeezed vacuum state (16), variations of the photon numbers for both the signal and idler fields are very small as the optical depth d is increased (solid blue lines). This is very different from the case with the use of the input of the single photon state (9), where the photon numbers of the two fields increase rapidly as d increases (dashed red lines). The physical reason for the very small variations of the photon numbers in both the signal and idler fields is due to the suppression of the K_- gain mode, by which the QVN and its amplification is largely inhibited in the system.

The fidelity is usually taken as a figure of merit for light propagation and for QM. Following the approach in Ref. [41],

we have carried out a detailed calculation on the fidelity of the photon propagation of the signal and idler pulses by taking the two-continuous-mode squeezed vacuum state (16) as an input. The result reads

$$F_{\text{SV}} = \exp\left(-\frac{L}{c} \int_{-\infty}^{+\infty} \frac{d\omega}{2\pi} \ln \frac{T}{4}\right), \quad (19a)$$

$$T = 4(1 + |X_{SI}|^2 + |X_{IS}|^2) \cosh^2(r) + W + \sinh(2r)(Ve^{i\theta} + V^*e^{-i\theta}), \quad (19b)$$

where $X_{SS} = C_{SS} \cosh(r) - C_{SI} \sinh(r) \exp(-i\theta)$, $X_{SI} = C_{SI} \cosh(r) - C_{SS} \exp(i\theta) \sinh(r)$, $X_{IS} = C_{IS} \cosh(r) - C_{II} \exp(-i\theta) \sinh(r)$, $X_{II} = C_{II} \cosh(r) - C_{IS} \exp(i\theta) \sinh(r)$, $V = X_{SS}^* X_{IS} + X_{II} X_{SI}^*$, and $W = 4|X_{SI}|^2 |X_{IS}|^2 - |V|^2$. Details of the derivation of the result (19) are presented in Appendix F 2.

Shown in Fig. 1(b) is the evolution of the fidelity of the photon state in the system as a function of the optical depth d . Illustrated by the solid blue line is the result of photon-state fidelity F^{SV} when the input is taken to be the two-continuous-mode squeezed vacuum state (16), while the dashed red line in the figure is the result of photon-state fidelity F^{SP} when the input is taken to be the single photon state (9). We see that, in comparison with the case of the single-photon input, the photon-state fidelity with the input of the two-continuous-mode squeezed vacuum state is much higher and it decreases much slower during propagation. This is also due to the suppression of the K_- gain mode, by which the QVN and its amplification is largely restrained and hence the photon-state fidelity during propagation is greatly improved.

V. SUMMARY

In this work, we have proposed a scheme for suppressing the quantum vacuum noise and its amplification for the photon propagation in a double- Λ atomic gas working on the conditions of EIT and FWM. Different from previous studies, we have presented a detailed analysis on the dispersion relations of the system, and have shown that the combined propagation of the signal and idler fields can be described by using two normal modes, i.e., the absorption normal mode and the gain normal mode, which have features of collective excitations. We have demonstrated that it is just the gain normal mode that brings gain to both the signal and idler fields and hence generates and amplifies the quantum noise in the system. Based on these results, we have suggested a method for suppressing the normal gain mode through the use of an input of two-continuous-mode squeezed vacuum state. Therefore, a significant suppression of the quantum noise and its amplification is realized and hence the fidelity of the photon propagation for both the signal and idler fields is largely improved.

The research results reported in this work are not only useful for the understanding of the physical property of the photon propagation in multilevel systems, but also helpful for further investigations on related topics of quantum information processing and transmission, including the high-fidelity propagation of atom-based squeezed lights, the improvement of the quality of multimode quantum memory, and so on.

ACKNOWLEDGMENTS

This work was supported by the National Natural Science Foundation of China under Grants No. 11474099 and No. 19975098.

APPENDIX A: EXPLICIT EXPRESSIONS OF THE HEISENBERG-LANGEVIN EQUATIONS

The explicit expressions of the equations of motion of the atomic-transition operators $\hat{S}_{\alpha\beta}$ (i.e., Heisenberg-Langevin equations) read

$$i\frac{\partial}{\partial t}\hat{S}_{11} - i\Gamma_{13}\hat{S}_{33} - i\Gamma_{14}\hat{S}_{44} + \Omega_{c2}^*\hat{S}_{14} - \Omega_{c2}\hat{S}_{41} + g_S^*\hat{a}_S^\dagger\hat{S}_{13} - g_S\hat{S}_{31}\hat{a}_S - i\hat{F}_{11} = 0, \quad (A1a)$$

$$i\frac{\partial}{\partial t}\hat{S}_{22} - i\Gamma_{23}\hat{S}_{33} - i\Gamma_{24}\hat{S}_{44} + \Omega_{c1}^*\hat{S}_{23} - \Omega_{c1}\hat{S}_{32} + g_I^*\hat{a}_I^\dagger\hat{S}_{24} - g_I\hat{S}_{42}\hat{a}_I - i\hat{F}_{22} = 0, \quad (A1b)$$

$$i\left(\frac{\partial}{\partial t} + \Gamma_3\right)\hat{S}_{33} + \Omega_{c1}\hat{S}_{32} - \Omega_{c1}^*\hat{S}_{23} + g_S\hat{S}_{31}\hat{a}_S - g_S^*\hat{a}_S^\dagger\hat{S}_{13} - i\hat{F}_{33} = 0, \quad (A1c)$$

$$i\left(\frac{\partial}{\partial t} + \Gamma_4\right)\hat{S}_{44} + \Omega_{c2}\hat{S}_{41} - \Omega_{c2}^*\hat{S}_{14} + g_I\hat{S}_{42}\hat{a}_I - g_I^*\hat{a}_I^\dagger\hat{S}_{24} - i\hat{F}_{44} = 0, \quad (A1d)$$

for diagonal elements, and

$$\left(i\frac{\partial}{\partial t} + d_{32}\right)\hat{S}_{23} + \Omega_{c1}(\hat{S}_{22} - \hat{S}_{33}) + g_S\hat{S}_{21}\hat{a}_S - g_I\hat{S}_{43}\hat{a}_I - i\hat{F}_{23} = 0, \quad (A2a)$$

$$\left(i\frac{\partial}{\partial t} + d_{41}\right)\hat{S}_{14} + \Omega_{c2}(\hat{S}_{11} - \hat{S}_{44}) - g_S\hat{S}_{34}\hat{a}_S + g_I\hat{S}_{12}\hat{a}_I - i\hat{F}_{14} = 0, \quad (A2b)$$

$$\left(i\frac{\partial}{\partial t} + d_{21}\right)\hat{S}_{12} + \Omega_{c1}^*\hat{S}_{13} - \Omega_{c2}\hat{S}_{42} - g_S\hat{S}_{32}\hat{a}_S + g_I^*\hat{a}_I^\dagger\hat{S}_{14} - i\hat{F}_{12} = 0, \quad (A2c)$$

$$\left(i\frac{\partial}{\partial t} + d_{31}\right)\hat{S}_{13} + \Omega_{c1}\hat{S}_{12} - \Omega_{c2}\hat{S}_{43} + g_S(\hat{S}_{11} - \hat{S}_{33})\hat{a}_S - i\hat{F}_{13} = 0, \quad (A2d)$$

$$\left(i\frac{\partial}{\partial t} + d_{24}\right)\hat{S}_{42} + \Omega_{c1}^*\hat{S}_{43} - \Omega_{c2}^*\hat{S}_{12} - g_I^*\hat{a}_I^\dagger(\hat{S}_{22} - \hat{S}_{44}) - i\hat{F}_{42} = 0, \quad (A2e)$$

$$\left(i\frac{\partial}{\partial t} + d_{34}\right)\hat{S}_{43} + \Omega_{c1}\hat{S}_{42} - \Omega_{c2}^*\hat{S}_{13} - g_I^*\hat{a}_I^\dagger\hat{S}_{23} + g_S\hat{S}_{41}\hat{a}_S - i\hat{F}_{43} = 0, \quad (A2f)$$

for nondiagonal elements, with $d_{\alpha\beta} = \Delta_\alpha - \Delta_\beta + i\gamma_{\alpha\beta}$, $\gamma_{\alpha\beta} = (\Gamma_\alpha + \Gamma_\beta)/2 + \gamma_{\alpha\beta}^{\text{dep}}$, and $\Gamma_\alpha = \sum_{E_\beta < E_\alpha} \Gamma_{\beta\alpha}$. Here $\Gamma_{\beta\alpha}$ is the spontaneous-emission rate from the state $|\alpha\rangle$ to the state $|\beta\rangle$; $\gamma_{\alpha\beta}^{\text{dep}}$ is the dephasing rate between the state $|\alpha\rangle$ and the state $|\beta\rangle$. Note that when writing the above equations

we have used the normal ordering of operators, i.e., the creation operators are always put on the left-handed side of the annihilation operators [61].

In Eqs. (A1) and (A2), $\hat{F}_{\alpha\beta}$ are δ -correlated Langevin noise operators, defined by $\hat{F}_{\alpha\beta} = N_z^{-1} \sum_{z_j \in \Delta_z} \hat{F}_{\alpha\beta}^j$, with $\hat{F}_{\alpha\beta}^j$ the Langevin noise operator of the atom at z_j [65]. Some δ -correlated functions for $\hat{F}_{\alpha\beta}$ are listed as follows:

$$\begin{aligned} \langle \hat{F}_{12}(z, t) \hat{F}_{21}(z', t') \rangle &= \mathcal{N}^{-1} \delta(z - z') \delta(t - t') \\ &\times [\Gamma_{12} \langle \hat{S}_{11}(z, t) \rangle \\ &+ \Gamma_{12} \langle \hat{S}_{22}(z, t) \rangle + \Gamma_{13} \langle \hat{S}_{33}(z, t) \rangle], \end{aligned} \quad (\text{A3a})$$

$$\begin{aligned} \langle \hat{F}_{13}(z, t) \hat{F}_{31}(z', t') \rangle &= \mathcal{N}^{-1} \delta(z - z') \delta(t - t') \\ &\times [\Gamma_3 \langle \hat{S}_{11}(z, t) \rangle + \Gamma_{12} \langle \hat{S}_{22}(z, t) \rangle \\ &+ \Gamma_{13} \langle \hat{S}_{33}(z, t) \rangle], \end{aligned} \quad (\text{A3b})$$

$$\langle \hat{F}_{21}(z, t) \hat{F}_{12}(z', t') \rangle = \mathcal{N}^{-1} \delta(z - z') \delta(t - t') \Gamma_{23} \langle \hat{S}_{33}(z, t) \rangle, \quad (\text{A3c})$$

$$\langle \hat{F}_{31}(z, t) \hat{F}_{13}(z', t') \rangle = 0. \quad (\text{A3d})$$

Their Fourier transformations are used in the calculation of the photon numbers of the two fields, as given by Eqs. (11) and (12).

APPENDIX B: ZERO-ORDER AND FIRST-ORDER SOLUTIONS OF THE HEISENBERG-LANGEVIN-MAXWELL EQUATIONS

1. Zero-order solution

The zero-order (i.e., base state) solution of the system is the steady-state solution of the Heisenberg-Langevin equation (3a) [or equivalently Eqs. (A1) and (A2)] when the signal and idler fields are absent (i.e., $\hat{a}_S = \hat{a}_I = 0$), which reads

$$\hat{S}_{11}^{(0)} = \frac{(\Gamma_4 + D_{41}) D_{32} \Gamma_{13}}{(\Gamma_3 + 2D_{32}) D_{41} \Gamma_{24} + (\Gamma_4 + 2D_{41}) D_{32} \Gamma_{13}} \hat{I}, \quad (\text{B1a})$$

$$\hat{S}_{22}^{(0)} = \frac{(\Gamma_3 + D_{32}) D_{41} \Gamma_{24}}{(\Gamma_3 + 2D_{32}) D_{41} \Gamma_{24} + (\Gamma_4 + 2D_{41}) D_{32} \Gamma_{13}} \hat{I}, \quad (\text{B1b})$$

$$\hat{S}_{33}^{(0)} = \frac{D_{32} D_{41} \Gamma_{24}}{(\Gamma_3 + 2D_{32}) D_{41} \Gamma_{24} + (\Gamma_4 + 2D_{41}) D_{32} \Gamma_{13}} \hat{I}, \quad (\text{B1c})$$

$$\hat{S}_{44}^{(0)} = \frac{D_{41} D_{32} \Gamma_{13}}{(\Gamma_3 + 2D_{32}) D_{41} \Gamma_{24} + (\Gamma_4 + 2D_{41}) D_{32} \Gamma_{13}} \hat{I}, \quad (\text{B1d})$$

$$\hat{S}_{23}^{(0)} = -\frac{\Omega_{c1}}{d_{32}} \frac{\Gamma_3 \Gamma_{24} D_{41}}{(\Gamma_3 + 2D_{32}) D_{41} \Gamma_{24} + (\Gamma_4 + 2D_{41}) D_{32} \Gamma_{13}} \hat{I}, \quad (\text{B1e})$$

$$\hat{S}_{14}^{(0)} = -\frac{\Omega_{c2}}{d_{41}} \frac{\Gamma_4 \Gamma_{13} D_{32}}{(\Gamma_3 + 2D_{32}) D_{41} \Gamma_{24} + (\Gamma_4 + 2D_{41}) D_{32} \Gamma_{13}} \hat{I}, \quad (\text{B1f})$$

with other $\hat{S}_{\alpha\beta}^{(0)} = 0$, where $\hat{I} = \sum_{\alpha=1}^4 |\alpha\rangle\langle\alpha|$ is the identity operator for atomic variables, $D_{32} = 2\gamma_{32}/|d_{32}|^2$, and $D_{41} = 2\gamma_{41}/|d_{41}|^2$. Note that, when obtaining the zero-order solution, we have assumed the Langevin noise is small, which will be included in the first-order approximation; see below.

Large Δ_4 approximation. If Δ_4 is very large, the zero-order solution is reduced into the simple form $\hat{S}_{11}^{(0)} \approx \hat{I}$, $\hat{S}_{14}^{(0)} \approx -\delta \hat{I}$ ($\delta \equiv \Omega_{c2}/\Delta_4 \ll 1$), with other $\hat{S}_{\alpha\beta}^{(0)} \approx 0$. That is to say, the atoms are mainly populated at the ground state $|1\rangle$, with only a very small amount of them populated in the state $|4\rangle$.

2. First-order solution

Assuming $\hat{S}_{\alpha\beta} \rightarrow \hat{S}_{\alpha\beta}^{(0)} + \hat{S}_{\alpha\beta}$, for small \hat{a}_S and \hat{a}_I Eq. (3a) can be linearized, with form given by

$$\left(i \frac{\partial}{\partial t} + d_{21} \right) \hat{S}_{12} + \Omega_{c1}^* \hat{S}_{13} - \Omega_{c2} \hat{S}_{42} - \delta g_I^* \hat{a}_I^\dagger - i \hat{F}_{12} = 0, \quad (\text{B2a})$$

$$\left(i \frac{\partial}{\partial t} + d_{31} \right) \hat{S}_{13} + \Omega_{c1} \hat{S}_{12} - \Omega_{c2} \hat{S}_{43} + g_S \hat{a}_S - i \hat{F}_{13} = 0, \quad (\text{B2b})$$

$$\left(i \frac{\partial}{\partial t} + d_{24} \right) \hat{S}_{42} + \Omega_{c1}^* \hat{S}_{43} - \Omega_{c2}^* \hat{S}_{12} - i \hat{F}_{42} = 0, \quad (\text{B2c})$$

$$\left(i \frac{\partial}{\partial t} + d_{34} \right) \hat{S}_{43} + \Omega_{c1} \hat{S}_{42} - \Omega_{c2}^* \hat{S}_{13} - \delta^* g_S \hat{a}_S - i \hat{F}_{43} = 0. \quad (\text{B2d})$$

We employ the Fourier transform

$$\hat{a}_S(z, t) = \frac{1}{\sqrt{2\pi}} \int_{-\infty}^{+\infty} d\omega \tilde{a}_S(z, \omega) e^{-i\omega t}, \quad (\text{B3a})$$

$$\hat{a}_I^\dagger(z, t) = \frac{1}{\sqrt{2\pi}} \int_{-\infty}^{+\infty} d\omega \tilde{a}_I^\dagger(z, \omega) e^{-i\omega t}, \quad (\text{B3b})$$

$$\hat{S}_{\alpha\beta}(z, t) = \frac{1}{\sqrt{2\pi}} \int_{-\infty}^{+\infty} d\omega \tilde{S}_{\alpha\beta}(z, \omega) e^{-i\omega t}, \quad (\text{B3c})$$

$$\hat{F}_{\alpha\beta}(z, t) = \frac{1}{\sqrt{2\pi}} \int_{-\infty}^{+\infty} d\omega \tilde{F}_{\alpha\beta}(z, \omega) e^{-i\omega t}, \quad (\text{B3d})$$

to solve Eq. (B2) and the Maxwell equations (3b) and (3c) under the large Δ_4 approximation. Then, we obtain the following relations:

$$\begin{aligned} \tilde{S}_{12} &\approx -\frac{\Omega_{c1}^*}{D} g_S \tilde{a}_S - \frac{\omega + D_{31}}{D} \delta g_I^* \tilde{a}_I^\dagger \\ &\quad - \frac{\omega + D_{31}}{D} i \tilde{F}_{12} + \frac{\Omega_{c1}^*}{D} i \tilde{F}_{13}, \end{aligned} \quad (\text{B4a})$$

$$\begin{aligned} \tilde{S}_{13} &\approx \frac{\omega + D_{21}}{D} g_S \tilde{a}_S + \frac{\Omega_{c1}}{D} \delta g_I^* \tilde{a}_I^\dagger \\ &\quad + \frac{\Omega_{c1}}{D} i \tilde{F}_{12} - \frac{\omega + D_{21}}{D} i \tilde{F}_{13}, \end{aligned} \quad (\text{B4b})$$

$$\tilde{S}_{42} \approx -\delta^* \tilde{S}_{12}, \quad (\text{B4c})$$

$$\tilde{S}_{43} \approx -\delta^* \tilde{S}_{13}, \quad (\text{B4d})$$

where $D(\omega) = |\Omega_{c1}|^2 - (\omega + D_{21})(\omega + D_{31})$ with $D_{\alpha 1} = d_{\alpha 1} + |\Omega_{c2}|^2/\Delta_4$. Note that, when deriving these relations, the terms proportional to and above δ^2 orders have been neglected. Substitution of these results into Eqs. (3b) and (3c) in the frequency domain yields the closed equations for \tilde{a}_S and \tilde{a}_I , i.e., Eq. (4) in the main text.

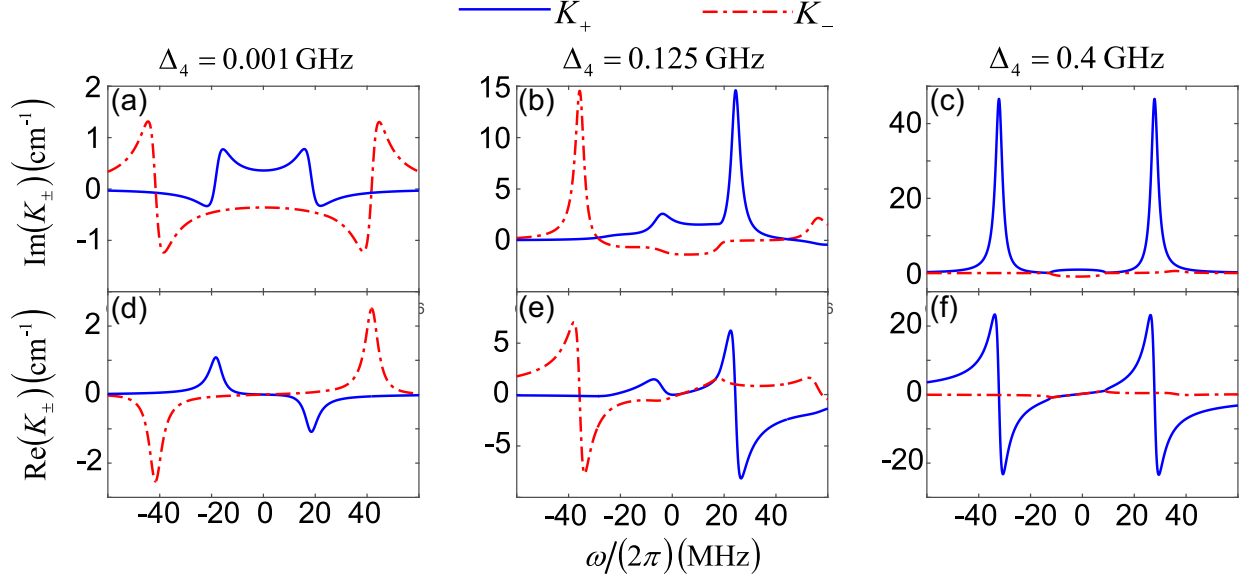


FIG. 6. Linear dispersion relations of the two normal modes K_+ and K_- as functions of ω for general value of Δ_4 . (a) Solid blue line is $\text{Im}(K_+)$ and dashed red line is $\text{Im}(K_-)$ for $\Delta_4 = 0.001$ GHz. (b) The same as (a) but for $\Delta_4 = 0.125$ GHz. (c) The same as (a) but for $\Delta_4 = 0.4$ GHz. (d) Solid blue line is $\text{Re}(K_+)$ and dashed red line is $\text{Re}(K_-)$ for $\Delta_4 = 0.001$ GHz. (e), (f) The same as (d) but for $\Delta_4 = 0.126$ GHz and $\Delta_4 = 0.4$ GHz, respectively.

APPENDIX C: SOLUTION OF EQ. (5) EXPRESSED BY QUANTITIES ON THE SYSTEM BOUNDARY

The solution given by Eq. (5) can also be expressed by the quantities on the system boundary $z = 0$, which reads [40,41]

$$\begin{aligned} \tilde{a}_S(z, \omega) &= C_{SS}(z, \omega)\tilde{a}_S(0, \omega) + C_{SI}(z, \omega)\tilde{a}_I^\dagger(0, \omega) \\ &+ \sqrt{\mathcal{N}} \int_0^z dz' [C_{S12}(z-z', \omega)\tilde{F}_{12}(z', \omega) \\ &+ C_{S13}(z-z', \omega)\tilde{F}_{13}(z', \omega)], \end{aligned} \quad (\text{C1a})$$

$$\begin{aligned} \tilde{a}_I^\dagger(z, \omega) &= C_{IS}(z, \omega)\tilde{a}_S(0, \omega) + C_{II}(z, \omega)\tilde{a}_I^\dagger(0, \omega) \\ &+ \sqrt{\mathcal{N}} \int_0^z dz' [C_{I12}(z-z', \omega)\tilde{F}_{12}(z', \omega) \\ &+ C_{I13}(z-z', \omega)\tilde{F}_{13}(z', \omega)], \end{aligned} \quad (\text{C1b})$$

with

$$C_{SS}(z, \omega) = \frac{G_-(\omega)e^{iK_+(\omega)z} - G_+(\omega)e^{iK_-(\omega)z}}{G_-(\omega) - G_+(\omega)}, \quad (\text{C2a})$$

$$C_{SI}(z, \omega) = \frac{e^{iK_+(\omega)z} - e^{iK_-(\omega)z}}{G_+(\omega) - G_-(\omega)}, \quad (\text{C2b})$$

$$C_{IS}(z, \omega) = G_+(\omega)G_-(\omega) \frac{e^{iK_+(\omega)z} - e^{iK_-(\omega)z}}{G_-(\omega) - G_+(\omega)}, \quad (\text{C2c})$$

$$C_{II}(z, \omega) = \frac{G_+(\omega)e^{iK_+(\omega)z} - G_-(\omega)e^{iK_-(\omega)z}}{G_+(\omega) - G_-(\omega)}, \quad (\text{C2d})$$

$$\begin{aligned} C_{S(I)12}(z, \omega) &= \sqrt{\mathcal{N}} \frac{(\omega + D_{31})\delta g_I C_{SI(I)}(z, \omega) - \Omega_{c1} g_S^* C_{SS(IS)}(z, \omega)}{D(\omega)}, \end{aligned} \quad (\text{C2e})$$

$$\begin{aligned} C_{S(I)13}(z, \omega) &= \sqrt{\mathcal{N}} \frac{(\omega + D_{21})g_S^* C_{SS(IS)}(z, \omega) - \Omega_{c1}^* \delta g_I C_{SI(I)}(z, \omega)}{D(\omega)}. \end{aligned} \quad (\text{C2f})$$

APPENDIX D: LINEAR DISPERSION RELATIONS OF THE TWO NORMAL MODES FOR GENERAL VALUE OF Δ_4

The consideration given in Fig. 2 and the related context are valid only for the special case of a large Δ_4 (i.e., $\Delta_4 = 2\pi \times 150$ MHz). It is natural to ask the question about the physical property of the two normal modes in the system if Δ_4 takes general values.

To answer this question, we have carried out a calculation on the zero-order and first-order solutions of the Heisenberg-Langevin-Maxwell Eqs. (3a)–(3c) for general Δ_4 . Shown in Fig. 6

is the linear dispersion relations of the two normal modes K_+ and K_- as functions of ω for several different values of Δ_4 . The solid blue line in panel (a) [(d)] is $\text{Im}(K_+)$ [$\text{Re}(K_+)$] and dashed red line is $\text{Im}(K_-)$ [$\text{Re}(K_-)$] for $\Delta_4 = 0.001$ GHz, with the other parameters the same as those used in Fig. 2. We see that for this small Δ_4 , which corresponds to a nearly resonant case, the K_+ mode displays an absorption [see panel (a)] and an abnormal dispersion [see panel (d)] with group-velocity $V_g^+|_{\omega=0} = -0.1353c$; the K_- -mode displays a gain [panel (a)] and a normal dispersion [panel (d)] with group-velocity $V_g^-|_{\omega=0} = 0.0894c$. Such result is very different from that shown in Fig. 2.

Shown in panels (b) and (e) are for the case with an intermediate value of Δ_4 (i.e., $\Delta_4 = 0.125$ GHz). As in panels (a) and (d), the solid blue line in panel (b) [(e)] is $\text{Im}(K_+)$ [$\text{Re}(K_+)$] and dashed red line is $\text{Im}(K_-)$ [$\text{Re}(K_-)$]. One sees

that in this case both the K_+ and K_- modes display very complicated behavior.

The case for $\Delta_4 = 0.4$ GHz corresponds to a far-off resonant case, with the property similar to that shown in Fig. 2. That is to say, a bubble region appears in panel (c) and coincidence straight lines appear in panel (f). Thus, near $\omega = 0$, the K_+ (K_-) mode has an absorption (a gain),

and both the K_+ and K_- modes display normal dispersion with group velocity $V_g^+|_{\omega=0} = V_g^-|_{\omega=0} = 0.0024 c$. By comparing with Fig. 2, one can deduce that, if Δ_4 is increased, the bubble region for $\text{Im}(K_+)$ [and also coincidence straight lines region for $\text{Im}(K_-)$] will be shrunken, which is due to the increased role played by EIT for increased Δ_4 .

APPENDIX E: PHOTON PROPAGATION WITH THE INPUT OF A PULSED TWO-CONTINUOUS-MODE SQUEEZED VACUUM STATE

The result given by (18) is valid only for the case where the two-continuous-mode squeezed vacuum state is prepared in a SPDC with a monochromatic pump beam. However, in many cases the pump beam in SPDC has a finite bandwidth, and due to the dispersion effect of the optical parametric oscillator the generated signal and the idler fields are pulsed [66]. Here, we consider the photon propagation with the pump beam in the SPDC has a finite bandwidth. In this situation, the two-continuous-mode squeezed vacuum state has the following form [58]:

$$|\Psi^{\text{SV}}\rangle = e^{\int_{-\infty}^{+\infty} d\omega \int_{-\infty}^{+\infty} d\omega' [\beta^*(\omega, \omega') \tilde{a}_S(0, \omega) \tilde{a}_I(0, \omega') - \beta(\omega, \omega') \tilde{a}_S^\dagger(0, \omega) \tilde{a}_I^\dagger(0, \omega')]} | \{0_S\}, \{0_I\} \rangle, \quad (\text{E1})$$

where $\beta(\omega, \omega')$ describes a wave packet of pair photon, with the first (second) argument ω (ω') denoting the sideband frequency component of the signal (idler) field. It is easy to deduce that the input state Eq. (E1) is reduced to Eq. (16) [58] when the pump beam is a monochromatic one (with angular frequency ω_c), because in this case one has $\beta(\omega, \omega') = \xi(\omega) \delta(\omega_S + \omega + \omega_I + \omega' - \omega_c) = \xi(\omega) \delta(\omega + \omega')$.

To study the photon propagation, here we consider a simple case by taking $\beta(\omega, \omega') = \xi(\omega) \delta_\Delta(\omega + \omega')$, where $\xi(\omega) = A \exp[-\omega^2/(2\omega_d^2)]$ and $\delta_\Delta(\omega + \omega') = (\sqrt{\pi} \Delta)^{-1} \exp[-(\omega + \omega')^2/\Delta^2]$ is a Gaussian function, which is close to the standard Dirac-delta function $\delta(\omega + \omega')$ if the parameter Δ is small. Because solving the problem exactly under the general input (E1) is rather cumbersome, we assume β is a small quantity (valid for the small photon number in the system), so that the solution of the problem can be obtained via a perturbation approach. Substituting the solution (5) [with (6)] and the general input state (E1) into the expression (17), we obtain $n_j^{\text{SV}}(z) = \int_{-\infty}^{+\infty} dt I_j^{\text{SV}}(z, t)$, where $I_j^{\text{SV}}(z, t) = I_{j1}^{\text{SV}}(z, t) + I_{j10}^{\text{SV}}(z, t)$ is the total photon flux of j th field ($j = S, I$). We get

$$\begin{aligned} I_{S1}^{\text{SV}}(z, t) \approx & \int_{-\infty}^{+\infty} d\omega' \left[\left| \int_{-\infty}^{+\infty} \frac{d\omega}{\sqrt{2\pi}} C_{SS}(z, \omega) \beta(\omega, \omega') e^{-i\omega t} \right|^2 + \left| \int_{-\infty}^{+\infty} \frac{d\omega}{\sqrt{2\pi}} C_{SI}(z, \omega) \beta^*(\omega', -\omega) e^{-i\omega t} \right|^2 \right] \\ & - \int_{-\infty}^{+\infty} \frac{d\omega}{\sqrt{2\pi}} \int_{-\infty}^{+\infty} \frac{d\omega'}{\sqrt{2\pi}} C_{SS}^*(z, \omega) C_{SI}(z, \omega') e^{i(\omega - \omega')t} \\ & \times \left[\beta^*(\omega, -\omega') + \frac{1}{2} \int_{-\infty}^{+\infty} d\omega'' \beta^*(\omega, \omega'') \int_{-\infty}^{+\infty} d\omega'_1 \beta^*(\omega'_1, -\omega') \beta(\omega'_1, \omega'') \right] \\ & - \int_{-\infty}^{+\infty} \frac{d\omega}{\sqrt{2\pi}} \int_{-\infty}^{+\infty} \frac{d\omega'}{\sqrt{2\pi}} C_{SI}^*(z, \omega) C_{SS}(z, \omega') e^{i(\omega - \omega')t} \\ & \times \left[\beta(\omega', -\omega) + \frac{1}{2} \int_{-\infty}^{+\infty} d\omega'_1 \beta(\omega'_1, -\omega) \int_{-\infty}^{+\infty} d\omega'' \beta(\omega'_1, \omega'') \beta^*(\omega', \omega'') \right], \end{aligned} \quad (\text{E2a})$$

$$I_{S10}^{\text{SV}}(z, t) = \int_{-\infty}^{+\infty} \frac{d\omega}{2\pi} |C_{SI}(z, \omega)|^2, \quad (\text{E2b})$$

$$\begin{aligned} I_{I1}^{\text{SV}}(z, t) \approx & \int_{-\infty}^{+\infty} d\omega' \left[\left| \int_{-\infty}^{+\infty} \frac{d\omega}{\sqrt{2\pi}} C_{IS}(z, \omega) \beta(\omega, \omega') e^{-i\omega t} \right|^2 + \left| \int_{-\infty}^{+\infty} \frac{d\omega}{\sqrt{2\pi}} C_{II}(z, \omega) \beta^*(\omega', -\omega) e^{-i\omega t} \right|^2 \right] \\ & - \int_{-\infty}^{+\infty} \frac{d\omega}{\sqrt{2\pi}} \int_{-\infty}^{+\infty} \frac{d\omega'}{\sqrt{2\pi}} C_{II}(z, \omega) C_{IS}^*(z, \omega') e^{-i(\omega - \omega')t} \\ & \times \left[\beta^*(\omega', -\omega) + \frac{1}{2} \int_{-\infty}^{+\infty} d\omega'_1 \beta^*(\omega'_1, -\omega) \int_{-\infty}^{+\infty} d\omega'' \beta^*(\omega', \omega'') \beta(\omega'_1, \omega'') \right] \\ & - \int_{-\infty}^{+\infty} \frac{d\omega}{\sqrt{2\pi}} \int_{-\infty}^{+\infty} \frac{d\omega'}{\sqrt{2\pi}} C_{IS}(z, \omega) C_{II}^*(z, \omega') e^{-i(\omega - \omega')t} \end{aligned}$$

$$\times \left[\beta(\omega, -\omega') + \frac{1}{2} \int_{-\infty}^{+\infty} d\omega'' \beta(\omega, \omega'') \int_{-\infty}^{+\infty} d\omega'_1 \beta^*(\omega'_1, \omega'') \beta(\omega'_1, -\omega') \right], \quad (\text{E2c})$$

$$I_{I10}^{\text{SV}}(z, t) = \int_{-\infty}^{+\infty} \frac{d\omega}{2\pi} |C_{IS}(z, \omega)|^2, \quad (\text{E2d})$$

where $I_{j1}^{\text{SV}}(z, t)$ is contributed by the nonzero input of both the signal and idler fields, $I_{j10}^{\text{SV}}(z, t)$ ($j = S, I$) comes from the QVN, and the expressions of C_{SI} , C_{SS} , C_{IS} , and C_{II} have been presented in Appendix C. When writing down the above result, the small contribution from the Langevin noise has been neglected.

Shown in Fig. 7(a) is the photon flux of the signal field (i.e., $I_S^{\text{SV}} \equiv I_{S1}^{\text{SV}} + I_{S10}^{\text{SV}}$) as a function of time t and the optical depth d , based on the result given by the expression (E2). The solid blue, red, and green lines are for $d = 0, 12$, and 24 , respectively. Figure 7(b) is the same as Fig. 7(a) but for the photon flux of the idler field, i.e., $I_I^{\text{SV}} \equiv I_{I1}^{\text{SV}} + I_{I10}^{\text{SV}}$. Illustrated in Fig. 7(c) is the photon number of the signal field $n_S^{\text{SV}}(z) = \int dt I_S^{\text{SV}}(z, t)$ as a function of d , with the input of the pulsed squeezed vacuum state (E1) (line 1: solid red line) and the continuous-wave squeezed vacuum state (16) (line 2: dashed blue line). Figure 7(d) is the same as Fig. 7(c) but for the photon number of the idler field $n_I^{\text{SV}}(z) = \int dt I_I^{\text{SV}}(z, t)$. When plotting this figure, we have taken $\Delta = 0.05\gamma_{31}$, $A = 1.0$, and $\omega_d = \gamma_{31}$.

From the figure, we see that during propagation the signal and idler pulses can keep their waveforms quite well, which is due to the effective cancellation of the gain mode K_- , by which the amplification of both fields is largely suppressed. However, the pulses are broadened and some sided components get increased, resulting from the later amplification

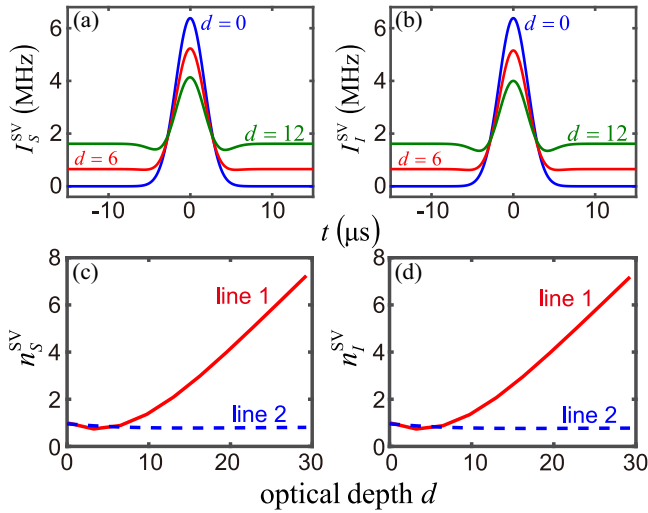


FIG. 7. (a) Photon flux of the signal field I_S^{SV} [with the input of the pulsed two-continuous-mode squeezed vacuum state (E1)] as a function of time t and the optical depth d . The solid blue, red, and green lines are for $d = 0, 6$, and 12 , respectively. (b) The same as (a) but for the photon flux of the idler field I_I^{SV} . (c) Photon number of the signal field n_S^{SV} as a function of d , with the input of the pulsed squeezed vacuum state (E1) (line 1: solid red line) and the continuous-wave squeezed vacuum state (16) (line 2: dashed blue line). (d) The same as (c) but for the photon number of the idler field n_I^{SV} .

of the photon numbers, which arise from the damping and the incomplete suppression of the quantum vacuum noise; in addition, when the photon number becomes large, higher-order terms in the perturbation calculation play roles and must be included in the calculation, and hence the result will be modified.

APPENDIX F: CALCULATING DETAIL ON THE FIDELITY OF PHOTON PROPAGATION

For an input pure state $|\Psi\rangle$, the fidelity of photon states is defined as the overlap integration between the input and output density matrices of the system, which reads $F \equiv \langle \Psi | \hat{\rho}_{\text{out}} | \Psi \rangle$. Following Ref. [41], we write the output density matrix $\hat{\rho}_{\text{out}}$ in a multimode Glauber-Sudarshan P representation, given by

$$\hat{\rho}_{\text{out}} = \prod_n \int_{-\infty}^{+\infty} \frac{d^2\alpha_{S,n}}{\pi} \int_{-\infty}^{+\infty} \frac{d^2\alpha_{I,-n}}{\pi} \times P(\{\alpha_S\}, \{\alpha_I\}) |\{\alpha_S\}, \{\alpha_I\}\rangle \langle \{\alpha_S\}, \{\alpha_I\}|, \quad (\text{F1})$$

with $d^2x \equiv d \text{Re}(x) d \text{Im}(x)$ hereafter. The quasiprobability distribution function $P(\{\alpha_S\}, \{\alpha_I\})$ is the inverse Fourier transform of the normally ordered characteristic function, given by

$$P(\{\alpha_S\}, \{\alpha_I\}) = \prod_n \int_{-\infty}^{+\infty} \frac{d^2\phi_{S,n}}{\pi} \int_{-\infty}^{+\infty} \frac{d^2\phi_{I,-n}}{\pi} \chi_N(\{\phi_S\}, \{\phi_I\}) \times \exp(\alpha_{S,n} \phi_{S,n}^* - \alpha_{S,n}^* \phi_{S,n}) \times \exp(\alpha_{I,-n} \phi_{I,-n}^* - \alpha_{I,-n}^* \phi_{I,-n}), \quad (\text{F2})$$

where the multimode characteristic function can be found from the trace over the density matrix, defined by [41,67]

$$\begin{aligned} \chi_N(\{\phi_S\}, \{\phi_I\}) &\equiv \langle \Psi | \exp \left\{ \sum_n [\phi_{S,n} \tilde{a}_{S,n}^\dagger(z) + \phi_{I,-n} \tilde{a}_{I,-n}^\dagger(z)] \right\} \\ &\times \exp \left\{ - \sum_n [\phi_{S,n}^* \tilde{a}_{S,n}(z) + \phi_{I,-n}^* \tilde{a}_{I,-n}(z)] \right\} | \Psi \rangle, \end{aligned} \quad (\text{F3})$$

with $\tilde{a}_{S,n}(z)$ and $\tilde{a}_{I,-n}^\dagger(z)$ the output solutions (C1) given in a discrete frequency form [i.e., $\tilde{a}(z, \omega) \rightarrow \tilde{a}_n(z)$], given by

$$\tilde{a}_{S,n}(z) = C_{SS,n}(z) \tilde{a}_{S,n}(0) + C_{SI,n}(z) \tilde{a}_{I,-n}^\dagger(0), \quad (\text{F4a})$$

$$\tilde{a}_{I,-n}^\dagger(z) = C_{IS,n}(z) \tilde{a}_{S,n}(0) + C_{II,n}(z) \tilde{a}_{I,-n}^\dagger(0), \quad (\text{F4b})$$

where the Langevin noise terms have been neglected under large Δ_4 approximation [41]. Thereby, the fidelity can be

written as

$$F = \prod_n \int_{-\infty}^{+\infty} \frac{d^2\alpha_{S,n}}{\pi} \int_{-\infty}^{+\infty} \frac{d^2\alpha_{I,-n}}{\pi} |\langle \Psi | \{\alpha_S\}, \{\alpha_I\} \rangle|^2 P(\{\alpha_S\}, \{\alpha_I\}), \tag{F5}$$

where the kernel $|\langle \Psi | \{\alpha_S\}, \{\alpha_I\} \rangle|^2$ is the overlap of the input state with the multimode coherent state. Below, we shall give details on the fidelity (F5) with the input state taken to be the single photon state (9) and the two-mode squeezed vacuum state (16) separately.

1. Fidelity for the input with the single photon state

For the single-photon state in a discrete frequency form, i.e., $|\Psi^{SP}\rangle = \sum_n f_{S,n} \hat{a}_{S,n}^\dagger(0) |0_S\rangle, |0_I\rangle$, the normally ordered characteristic function $\chi_N(\{\phi_S\}, \{\phi_I\})$ is explicitly given by

$$\begin{aligned} \chi_N &= \left[1 - \left| \sum_j f_{S,j} (\phi_{S,j}^* C_{SS,j} - \phi_{I,-j} C_{IS,j}) \right|^2 \right] \\ &\times \prod_n \exp \left[-|C_{SI,n}|^2 |\phi_{S,n}|^2 - |C_{IS,n}|^2 |\phi_{I,-n}|^2 + \frac{U_n}{2} \phi_{S,n} \phi_{I,-n} + \frac{U_n^*}{2} \phi_{S,n}^* \phi_{I,-n}^* \right], \end{aligned} \tag{F6}$$

where $U_n = C_{SS,n}^* C_{IS,n} + C_{SI,n}^* C_{II,n}$. The quasiprobability distribution function $P(\{\alpha_S\}, \{\alpha_I\})$ reads

$$\begin{aligned} P &= \prod_n \frac{4}{M_n} \exp \left(-\frac{4|C_{SI,n}|^2 |\alpha_{I,-n}|^2 + 4|C_{IS,n}|^2 |\alpha_{S,n}|^2 - 2U_n \alpha_{S,n} \alpha_{I,-n} - 2U_n^* \alpha_{S,n}^* \alpha_{I,-n}^*}{M_n} \right) \\ &\times \left[1 - 2 \sum_j |f_{S,j}|^2 \frac{2|C_{SS,j}|^2 |C_{IS,j}|^2 + 2|C_{IS,j}|^2 |C_{SI,j}|^2 - C_{SS,j}^* C_{IS,j} U_j^* - C_{SS,j} C_{IS,j}^* U_j}{M_j} \right. \\ &\left. + 4 \left| \sum_j f_{S,j} \frac{(2|C_{SI,j}|^2 C_{IS,j} - C_{SS,j} U_j) \alpha_{I,-j} + (2C_{SS,j} |C_{IS,j}|^2 - C_{IS,j} U_j^*) \alpha_{S,j}^*}{M_j} \right|^2 \right], \end{aligned} \tag{F7}$$

where $M_n = 4|C_{SI,n}|^2 |C_{IS,n}|^2 - |U_n|^2$.

Then, with the kernel in (F5) given by

$$|\langle \Psi^{SP} | \{\alpha_S\}, \{\alpha_I\} \rangle|^2 = \prod_n \exp [-(|\alpha_{S,j}|^2 + |\alpha_{I,-j}|^2)] \left| \sum_j f_{S,j} \alpha_{S,j}^* \right|^2, \tag{F8}$$

we can finally obtain the fidelity for the input single photon state, given by

$$F_{SP} = F_0 [4|F_1|^2 + F_2(1 - 2F_3)], \tag{F9a}$$

$$\begin{aligned} F_0 &= \prod_n \frac{4}{4 + 4|C_{SI,n}|^2 + 4|C_{IS,n}|^2 + M_n} = \exp \left\{ -\sum_n \ln \left(1 + |C_{SI,n}|^2 + |C_{IS,n}|^2 + \frac{M_n}{4} \right) \right\} \\ &\rightarrow \exp \left\{ -\frac{L}{c} \int \frac{d\omega}{2\pi} \ln \left(1 + |C_{SI}|^2 + |C_{IS}|^2 + \frac{M}{4} \right) \right\}, \end{aligned} \tag{F9b}$$

$$\begin{aligned} F_1 &= \sum_n |f_{S,n}|^2 \frac{2(|C_{IS,n}|^2 + 1)C_{SS,n}^* - C_{IS,n}^* U_n}{4 + 4|C_{SI,n}|^2 + 4|C_{IS,n}|^2 + M_n} \\ &\rightarrow \int d\omega |f_S|^2 \frac{2(|C_{IS}|^2 + 1)C_{SS}^* - C_{IS}^* U}{4 + 4|C_{SI}|^2 + 4|C_{IS}|^2 + M}, \end{aligned} \tag{F9c}$$

$$F_2 = \sum_n \frac{|f_{S,n}|^2 (4|C_{SI,n}|^2 + M_n)}{4 + 4|C_{SI,n}|^2 + 4|C_{IS,n}|^2 + M_n} \rightarrow \int d\omega \frac{|f_S(\omega)|^2 (4|C_{SI}|^2 + M)}{4 + 4|C_{SI}|^2 + 4|C_{IS}|^2 + M}, \tag{F9d}$$

$$\begin{aligned} F_3 &= \sum_n |f_{S,n}|^2 \frac{2(|C_{IS,n}|^2 + 1)|C_{SS,n}|^2 + 2(|C_{SI,n}|^2 + 1)|C_{IS,n}|^2 - C_{SS,n} C_{IS,n}^* U_n - C_{SS,n}^* C_{IS,n} U_n^*}{4 + 4|C_{SI,n}|^2 + 4|C_{IS,n}|^2 + M_n} \\ &\rightarrow \int d\omega |f_S|^2 \frac{2(|C_{IS}|^2 + 1)|C_{SS}|^2 + 2(|C_{SI}|^2 + 1)|C_{IS}|^2 - C_{SS} C_{IS}^* Z - C_{SS}^* C_{IS} Z^*}{4 + 4|C_{SI}|^2 + 4|C_{IS}|^2 + M}. \end{aligned} \tag{F9e}$$

In Eq. (F9), the summation on the discrete modes has been converted into integrals over continuous modes, i.e., $\sum_n \rightarrow L/(2\pi c) \int d\omega$. Similar to the results obtained in Ref. [41], the expression for the fidelity of the photon state is composed of two parts—a product F_0 multiplied by summations F_j ($j = 1, 2, 3$). The product can be interpreted as the vacuum contribution, since it is present even for the zero input of the signal and the idler fields. The summation is due to the nonzero input of the two fields. In order to compare with the case with the input two-mode squeezed vacuum state, the combined fidelity of both the signal and idler fields is considered for the case with the input single-photon state. Thus the approach presented here is little different from that given in Ref. [41], where only the fidelity of the signal field was calculated, through tracing over the counterpart for the idler field.

2. Fidelity for the input with the two-continuous-mode squeezed vacuum state

In this case, the discrete form of the input photon state reads $|\Psi^{\text{SV}}\rangle = \exp[\sum_n \xi_n^* \tilde{a}_{S,n}(0) \tilde{a}_{I,-n}(0) - \sum_n \xi_n \tilde{a}_{S,n}^\dagger(0) \tilde{a}_{I,-n}^\dagger(0)]|0_S\rangle, |0_I\rangle$; the normally ordered characteristic function $\chi_N(\{\phi_S\}, \{\phi_I\})$ is given by

$$\chi_N = \prod_n \exp\left(-|X_{SI,n}|^2 |\phi_{S,n}|^2 - |X_{IS,n}|^2 |\phi_{I,-n}|^2 + \frac{V_n}{2} \phi_{S,n} \phi_{I,-n} + \frac{V_n^*}{2} \phi_{S,n}^* \phi_{I,-n}^*\right), \quad (\text{F10})$$

where $V_n = X_{SS,n}^* X_{IS,n} + X_{II,n} X_{SI,n}^*$, with $X_{SS,n} = C_{SS,n} \cosh(r_n) - C_{SI,n} \exp(-i\theta_n) \sinh(r_n)$, $X_{SI,n} = C_{SI,n} \cosh r_n - C_{SS,n} \exp(i\theta_n) \sinh r_n$, $X_{IS,n} = C_{IS,n} \cosh r_n - C_{II,n} \exp(-i\theta_n) \sinh r_n$, and $X_{II,n} = C_{II,n} \cosh(r_n) - C_{IS,n} \exp(i\theta_n) \sinh(r_n)$. By virtue of these results, we obtain the quasiprobability distribution function $P(\{\alpha_S\}, \{\alpha_I\})$

$$P = \prod_n \frac{4}{W_n} \exp\left(-\frac{4|X_{SI,n}|^2 |\alpha_{I,-n}|^2 + 4|X_{IS,n}|^2 |\alpha_{S,n}|^2 - 2V_n \alpha_{S,n} \alpha_{I,-n} - 2V_n^* \alpha_{S,n}^* \alpha_{I,-n}^*}{W_n}\right), \quad (\text{F11})$$

with $W_n = 4|X_{SI,n}|^2 |X_{IS,n}|^2 - |V_n|^2$.

Then, with the kernel given by

$$|\langle \Psi_{\text{SV}} | \{\alpha_S\}, \{\alpha_I\} \rangle|^2 = \prod_n \text{sech}^2(r_n) \exp[-(|\alpha_{S,n}|^2 + |\alpha_{I,-n}|^2)] \exp[-\tanh(r_n)(e^{i\theta_n} \alpha_{S,n}^* \alpha_{I,-n}^* + e^{-i\theta_n} \alpha_{S,n} \alpha_{I,-n})], \quad (\text{F12})$$

the fidelity for the input two-mode squeezed vacuum state reads

$$F_{\text{SV}} = \prod_n \frac{4}{4(1 + |X_{SI,n}|^2 + |X_{IS,n}|^2) \cosh^2(r_n) + W_n + \sinh(2r_n)(V_n e^{i\theta_n} + V_n^* e^{-i\theta_n})}. \quad (\text{F13})$$

Based on this, we obtain its continuous limit form, which is given by Eq. (19) in the main text.

Note that, different from the result obtained for the case with the input single-photon state [given by Eq. (F9)], the fidelity F_{SV} for the case with the input two-mode squeezed vacuum state is a product of different modes, and is dependent on the input distribution function $\xi(\omega) = r(\omega) \exp[i\theta(\omega)]$. From this product we see that, on the one hand, the input two-mode squeezed vacuum state modifies the original QVN term [i.e., F_0 given by Eq. (F9)]; on the other hand, the QVN term involves an inseparable part of the input two-mode squeezed vacuum field and hence one cannot plot a figure (like Fig. 3) to illustrate the various photon numbers contributed by the nonzero input fields, Langevin noise, QVN, etc.

-
- [1] A. I. Lvovsky, B. C. Sanders, and W. Tittel, Optical quantum memory, *Nat. Photonics* **3**, 706 (2009).
- [2] C. Simon, M. Afzelius, J. Appe, A. B. Gero-day, S. J. Dewhurst, N. Gisin, C. Hu, F. Jelezko, S. Kröll, J. Müller, J. Nunn, E. Polzik, J. Rarity, H. Riedmatten, W. Rosenfeld, A. J. Shields, N. Sköld, R. M. Stevenson, R. Thew, I. Walmsley, M. Weber, H. Weinfurter, J. Wrachtrup, and R. J. Young, Quantum memories, *Euro. Phys. J. D* **58**, 1 (2010).
- [3] N. Sangouard, C. Simon, H. de Riedmatten, and N. Gisin, Quantum repeaters based on atomic ensembles and linear optics, *Rev. Mod. Phys.* **83**, 33 (2011).
- [4] F. Bussiè-res, N. Sangouard, M. Afzelius, H. de Riedmatten, C. Simon, and W. Tittel, Prospective applications of optical quantum memories, *J. Mod. Opt.* **60**, 1519 (2013).
- [5] K. Heshami, D. G. England, P. C. Humphreys, P. J. Bustard, V. M. Acosta, J. Nunn, and B. J. Sussman, Quantum memories: emerging applications and recent advances, *J. Mod. Opt.* **63**, 2005 (2016).
- [6] M. Fleischhauer, A. Imamoglu, and J. P. Marangos, Electromagnetically induced transparency: Optics in coherent media, *Rev. Mod. Phys.* **77**, 633 (2005).
- [7] M. Fleischhauer and M. D. Lukin, Dark-State-Polaritons in Electromagnetically Induced Transparency, *Phys. Rev. Lett.* **84**, 5094 (2000).
- [8] C. Liu, Z. Dutton, C. H. Behroozi, and L. V. Hau, Observation of coherent optical information storage in an atomic medium using halted light pulses, *Nature (London)* **409**, 490 (2001).
- [9] D. F. Phillips, A. Fleischhauer, A. Mair, R. L. Walsworth, and M. D. Lukin, Storage of Light in Atomic Vapor, *Phys. Rev. Lett.* **86**, 783 (2001).

- [10] N. B. Phillips, A. V. Gorshkov, and I. Novikova, Optimal light storage in atomic vapor, *Phys. Rev. A* **78**, 023801 (2008).
- [11] U. Schnorrberger, J. D. Thompson, S. Trotzky, R. Pugatch, N. Davidson, S. Kuhr, and I. Bloch, Electromagnetically Induced Transparency and Light Storage in an Atomic Mott Insulator, *Phys. Rev. Lett.* **103**, 033003 (2009).
- [12] I. Novikova, R. L. Walsworth, and Y. Xiao, Electromagnetically induced transparency-based slow and stored light in warm atoms, *Laser Photonics Rev.* **6**, 333 (2012).
- [13] Y.-H. Chen, M.-J. Lee, I.-C. Wang, S. Du, Y.-F. Chen, Y.-C. Chen, and I. A. Yu, Coherent Optical Memory with High Storage Efficiency and Large Fractional Delay, *Phys. Rev. Lett.* **110**, 083601 (2013).
- [14] Y. O. Dudin, L. Li, and A. Kuzmich, Light storage on the time scale of a minute, *Phys. Rev. A* **87**, 031801 (2013).
- [15] G. Heinze, C. Hubrich, and T. Halfmann, Stopped Light and Image Storage by Electromagnetically Induced Transparency Up to the Regime of One Minute, *Phys. Rev. Lett.* **111**, 033601 (2013).
- [16] Y. Chen, Z. Bai, and G. Huang, Ultraslow optical solitons and their storage and retrieval in an ultracold ladder-type atomic system, *Phys. Rev. A* **89**, 023835 (2014).
- [17] N. Sibalić, J. M. Kondo, C. S. Adams, and K. J. Weatherill, Dressed-state electromagnetically induced transparency for light storage in uniform-phase spin waves, *Phys. Rev. A* **94**, 033840 (2016).
- [18] Y.-F. Hsiao, P.-J. Tsai, H.-S. Chen, S.-X. Lin, C.-C. Hung, C.-H. Lee, Y.-H. Chen, Y.-F. Chen, I.-A. Yu, and Y.-C. Chen, Highly Efficient Coherent Optical Memory Based on Electromagnetically Induced Transparency, *Phys. Rev. Lett.* **120**, 183602 (2018).
- [19] G. Hétet, A. Peng, M. T. Johnsson, J. J. Hope, and P. K. Lam, Characterization of electromagnetically-induced-transparency-based continuous-variable quantum memories, *Phys. Rev. A* **77**, 012323 (2008).
- [20] J. Appel, E. Figueroa, D. Korystov, M. Lobino, and A. I. Lvovsky, Quantum Memory for Squeezed Light, *Phys. Rev. Lett.* **100**, 093602 (2008).
- [21] K. Honda, D. Akamatsu, M. Arikawa, Y. Yokoi, K. Akiba, S. Nagatsuka, T. Tanimura, A. Furusawa, and M. Kozuma, Storage and Retrieval of a Squeezed Vacuum, *Phys. Rev. Lett.* **100**, 093601 (2008).
- [22] H. Zhang *et al.*, Preparation and storage of frequency-uncorrelated entangled photons from cavity-enhanced spontaneous parametric downconversion, *Nat. Photonics* **5**, 628 (2011).
- [23] D.-S. Ding, Z.-Y. Zhou, B.-S. Shi, and G.-C. Guo, Single-photon-level quantum image memory based on cold atomic ensembles, *Nat. Commun.* **4**, 2527 (2013).
- [24] D. Maxwell, D. J. Szwer, D. Paredes-Barato, H. Busche, J. D. Pritchard, A. Gauguet, K. J. Weatherill, M. P. A. Jones, and C. S. Adams, Storage and Control of Optical Photons Using Rydberg Polaritons, *Phys. Rev. Lett.* **110**, 103001 (2013).
- [25] L. Li and A. Kuzmich, Quantum memory with strong and controllable Rydberg-level interactions, *Nat. Commun.* **7**, 13618 (2016).
- [26] S. J. Yang, J. Rui, H. N. Dai, X. M. Jin, S. Chen, and J.-W. Pan, High-contrast transparency comb of the electromagnetically-induced-transparency memory, *Phys. Rev. A* **98**, 033802 (2018).
- [27] B. Jing, X.-J. Wang, Y. Yu, P.-F. Sun, Y. Jiang, S. J. Yang, W. H. Jiang, X. Y. Luo, J. Zhang, X. Jiang, X.-H. Bao, and J.-W. Pan, Entanglement of three quantum memories via interference of three single photons, *Nat. Photonics* **13**, 210 (2019).
- [28] Y. Wang, J. Li, S. Zhang, K. Su, Y. Zhou, K. Liao, S. Du, H. Yan, and S.-L. Zhu, Efficient quantum memory for single-photon polarization qubits, *Nat. Photonics* **13**, 346 (2019).
- [29] A. S. Zibrov, A. B. Matsko, O. Kocharovskaya, Y. V. Rostovtsev, G. R. Welch, and M. O. Scully, Transporting and Time Reversing Light via Atomic Coherence, *Phys. Rev. Lett.* **88**, 103601 (2002).
- [30] A. Raczynski and J. Zaremba, Controlled light storage in a double lambda system, *Opt. Commun.* **209**, 149 (2002).
- [31] A. Raczynski and J. Zaremba, Electromagnetically induced transparency and storing of a pair of pulses of light, *Phys. Rev. A* **69**, 043801 (2004).
- [32] Z. Li, L. Xu, and K. Wang, The dark-state polaritons of a double- Λ atomic ensemble, *Phys. Lett. A* **346**, 269 (2005).
- [33] X.-J. Liu, H. Jing, and M.-L. Ge, Quantum memory process with a four-level atomic ensemble, *Euro. Phys. J. D* **40**, 297 (2006).
- [34] A. Eilam, A. D. Wilson-Gordon, and H. Friedmann, Slow and stored light in an amplifying double- Λ system, *Opt. Lett.* **33**, 1605 (2008).
- [35] P. K. Vudyasetu, R. M. Camacho, and J. C. Howell, Storage and Retrieval of Multimode Transverse Images in Hot Atomic Rubidium Vapor, *Phys. Rev. Lett.* **100**, 123903 (2008).
- [36] R. M. Camacho, P. K. Vudyasetu, and J. C. Howell, Four-wave-mixing stopped light in hot atomic rubidium vapour, *Nat. Photonics* **3**, 103 (2009).
- [37] D. Viscor, V. Ahufinger, J. Mompert, A. Zavatta, G. C. La Rocca, and M. Artoni, Two-color quantum memory in double- Λ media, *Phys. Rev. A* **86**, 053827 (2012).
- [38] J. Wu, Y. Liu, D.-S. Ding, Z.-Y. Zhou, B.-S. Shi, and G.-C. Guo, Light storage based on four-wave mixing and electromagnetically induced transparency in cold atoms, *Phys. Rev. A* **87**, 013845 (2013).
- [39] J. Geng, G. T. Campbell, J. Bernu, D. B. Higginbottom, B. M. Sparkes, S. M. Assad, W. P. Zhang, N. P. Robins, P. K. Lam, and B. C. Buchler, Electromagnetically induced transparency and four-wave mixing in a cold atomic ensemble with large optical depth, *New J. Phys.* **16**, 113053 (2014).
- [40] N. B. Phillips, A. V. Gorshkov, and I. Novikova, Light storage in an optically thick atomic ensemble under conditions of electromagnetically induced transparency and four-wave mixing, *Phys. Rev. A* **83**, 063823 (2011).
- [41] N. Lauk, C. O' Brien, and M. Fleischhauer, Fidelity of photon propagation in electromagnetically induced transparency in the presence of four-wave mixing, *Phys. Rev. A* **88**, 013823 (2013).
- [42] Although the analysis presented in Ref. [41] is given for the photon propagation in an EIT-based four-level atomic gas with a zero input of the idler laser field, the conclusion on the QVN generation obtained is valid also for the case with a nonzero input of the idler field.
- [43] D. Xu, C. Hang, and G. Huang, Improvement of the memory quality of optical pulse pairs in atomic systems via four-wave mixing, *Phys. Rev. A* **98**, 043848 (2018).
- [44] P. Walther, M. D. Eisaman, A. André, F. Massou, M. Fleischhauer, A. S. Zibrov, and M. D. Lukin, Generation of narrow-bandwidth single photons using electromagnetically

- induced transparency in atomic ensembles, *Int. J. Quantum Inf.* **5**, 51 (2007).
- [45] I. Vurgaftman and M. Bashkansky, Suppressing four-wave mixing in warm-atomic-vapor quantum memory, *Phys. Rev. A* **87**, 063836 (2013).
- [46] K. Zhang, J. Guo, L. Q. Chen, C. Yuan, Z. Y. Ou, and W. Zhang, Suppression of the four-wave-mixing background noise in a quantum memory retrieval process by channel blocking, *Phys. Rev. A* **90**, 033823 (2014).
- [47] G. Romanov, C. O. Brien, and I. Novikova, Suppression of the four-wave mixing amplification via Raman absorption, *J. Mod. Opt.* **63**, 2048 (2016).
- [48] D. J. Saunders, J. H. D. Munns, T. F. M. Champion, C. Qiu, K. T. Kaczmarek, E. Poem, P. M. Ledingham, I. A. Walmsley, and J. Nunn, Cavity-Enhanced Room-Temperature Broadband Raman Memory, *Phys. Rev. Lett.* **116**, 090501 (2016).
- [49] J. Nunn, J. H. D. Munns, S. Thomas, K. T. Kaczmarek, C. Qiu, A. Feizpour, E. Poem, B. Brecht, D. J. Saunders, P. M. Ledingham, D. V. Reddy, M. G. Raymer, and I. A. Walmsley, Theory of noise suppression in Λ -type quantum memories by means of a cavity, *Phys. Rev. A* **96**, 012338 (2017).
- [50] For simplicity, we assume that the signal and idler fields are wide enough in the transverse (i.e., x and y) directions, so that the diffraction effect is negligible.
- [51] D. A. Steck, Rubidium 87 D Line Data, <http://steck.us/alkalidata/>.
- [52] ω is the frequency deviation (sideband) of the signal and idler pulses from their central frequencies, resulted by the interaction with the atomic gas. Thus the frequency of the signal (idler) pulse in the atomic medium is given by $\omega_S + \omega$ ($\omega_I + \omega$).
- [53] The properties of the linear dispersion relation of the system described here have been verified by the use of Kramers-Kronig relations.
- [54] V. Balić, D. A. Braje, P. Kolchin, G. Y. Yin, and S. E. Harris, Generation of Paired Photons with Controllable Waveforms, *Phys. Rev. Lett.* **94**, 183601 (2005).
- [55] P. Kolchin, S. Du, C. Belthangady, G. Y. Yin, and S. E. Harris, Generation of Narrow-Bandwidth Paired Photons: Use of a Single Driving Laser, *Phys. Rev. Lett.* **97**, 113602 (2006).
- [56] S. Du, P. Kolchin, C. Belthangady, G. Y. Yin, and S. E. Harris, Subnatural Linewidth Biphotons with Controllable Temporal Length, *Phys. Rev. Lett.* **100**, 183603 (2008).
- [57] L. Zhao, X. Guo, C. Liu, Y. Sun, M. M. T. Loy, and S. Du, Photon pairs with coherence time exceeding $1 \mu\text{s}$, *Optica* **1**, 84 (2014).
- [58] R. Loudon, *The Quantum Theory of Light* (Oxford University Press, New York, 2000).
- [59] The origin of the QVN in the signal and idler fields is resulted from the Heisenberg commutation relations of the signal and idler signal field operators \tilde{a}_S and \tilde{a}_I , i.e., $[\tilde{a}_{S(I)}(z, \omega), \tilde{a}_{S(I)}^\dagger(z, \omega')] = \delta(\omega - \omega')$. Note that the QVN in the signal (idler) field may appear even when there is no input of the idler (signal) field. The QVN must be suppressed in systems required for working at single-photon level (such as single-photon memory) [41].
- [60] For clarity, “two-mode” here means two field modes (i.e., the signal field and the idler field) for a given ω .
- [61] M. O. Scully and M. S. Zubairy, *Quantum Optics* (Cambridge University Press, Cambridge, UK, 1997).
- [62] The two-mode squeezed vacuum state is defined by $|\xi\rangle \equiv r \exp(i\theta)|\rangle = \exp(\xi\hat{a}^\dagger\hat{b}^\dagger - \xi^*\hat{a}\hat{b})|0_a, 0_b\rangle$, satisfying the eigen-equation $[\hat{b}^\dagger + \coth r \exp(-i\theta)\hat{a}]|\xi\rangle = 0$, where \hat{a} and \hat{b} are annihilation operators of photons from two different light fields; $|0_a, 0_b\rangle \equiv |0_a\rangle \otimes |0_b\rangle$ is a two-mode vacuum state [58,61].
- [63] Here “two-continuous-mode” means that the quantum state of the squeezed vacuum contains two different light fields (i.e., the signal field and the idler field), with each being a wave packet having a continuous ω distribution [58].
- [64] Generally, the pump beam in the SPDC has a finite bandwidth. The calculation on the photon propagation in the system for such a situation is presented in Appendix E.
- [65] P. Kolchin, Electromagnetically-induced-transparency-based paired photon generation, *Phys. Rev. A* **75**, 033814 (2007).
- [66] To interface with the atomic gases, the bandwidth of the input signal and idler fields generated by SPDC must be narrowed, which can be realized by using an optical cavity [Z. Y. Ou and Y. J. Lu, *Phys. Rev. Lett.* **83**, 2556 (1999)]. Narrow-band signal and idler fields can also be obtained by means of spontaneous FWM; see, e.g., C.-S. Chuu and S. Du, Narrowband biphotons: Generation, manipulation, and applications, [arXiv:1503.04339v1](https://arxiv.org/abs/1503.04339v1), and U. L. Andersen, T. Gehring, C. Marquardt, and G. Leuchs, 30 years of squeezed light generation, *Phys. Scr.* **91**, 053001 (2016).
- [67] J. G. Garrison and R. Y. Chiao, *Quantum Optics* (Oxford University Press, New York, 2008).